

Lindblad many-body scars

Antonio M. García-García,^{1,*} Zhongling Lu,^{1,2,†} Lucas Sá,^{3,‡} and Jacobus J. M. Verbaarschot^{4,§}

¹*Shanghai Center for Complex Physics, School of Physics and Astronomy,
Shanghai Jiao Tong University, Shanghai 200240, China*

²*Zhiyuan College, Shanghai Jiao Tong University, Shanghai 200240, China*

³*TCM Group, Cavendish Laboratory, University of Cambridge, JJ Thomson Avenue, Cambridge CB3 0HE, UK*

⁴*Center for Nuclear Theory and Department of Physics and Astronomy,
Stony Brook University, Stony Brook, New York 11794, USA*

(Dated: March 11, 2025)

Quantum many-body scars have received much recent attention for being both intriguing non-ergodic states in otherwise quantum chaotic systems and promising candidates to encode quantum information efficiently. So far, these studies have mostly been restricted to Hermitian systems. Here, we study many-body scars in many-body quantum chaotic systems coupled to a Markovian bath, which we term Lindblad many-body scars. They are defined as simultaneous eigenvectors of the Hamiltonian and dissipative parts of the vectorized Liouvillian. Importantly, because their eigenvalues are purely real, they are not related to revivals. The number and nature of the scars depend on both the symmetry of the Hamiltonian and the choice of jump operators. For a dissipative four-body Sachdev-Ye-Kitaev (SYK) model with N fermions, either Majorana or complex, we construct analytically some of these Lindblad scars while others could only be obtained numerically. As an example of the former, we identify $N/2 + 1$ scars for complex fermions due to the $U(1)$ symmetry of the model and two scars for Majorana fermions as a consequence of the parity symmetry. Similar results are obtained for a dissipative XXZ spin chain. We also characterize the physical properties of Lindblad scars. First, the operator size is independent of the disorder realization and has a vanishing variance. By contrast, the operator size for non-scarred states, believed to be quantum chaotic, is well described by a distribution centered around a specific size and a finite variance, which could be relevant for a precise definition of the eigenstate thermalization hypothesis in dissipative quantum chaos. Moreover, the entanglement entropy of these scars has distinct features such as a strong dependence on the partition choice and, in certain cases, a large entanglement.

I. INTRODUCTION

Quantum scars [1], originally discovered forty years ago, are eigenstates of quantum chaotic systems whose wave functions are strongly localized along an unstable periodic orbit. The initial concept of quantum scars emerged from the studies of classical-quantum correspondence in single-particle systems, such as quantum billiards, which exhibit distinct semiclassical limits and have been directly observed [2] in experiments. More recently, the study of scars has received an important boost in the context of many-body quantum systems. In this case, due to the absence of a clear semiclassical characterization (see, however, Refs. [3–9] for recent developments along this line), quantum many-body scars [10–14] were identified, both theoretically and experimentally, by non-thermal oscillatory dynamics for some specific initial conditions related to the existence of towers of states with an equally spaced spectrum.

More generally, many-body scar states can be defined as analytical eigenstates of a system. Typically, one observes the coexistence of eigenstates that are given by an

explicit analytical expression, and eigenstates that can only be obtained numerically which show typical characteristics of chaotic states such as avoided level crossings and eigenstate thermalization. The coexistence of these two types of states was first identified in three- and four-anyon systems in a harmonic well [15–17], while the discovery of integrable many-anyon states goes back much further [18]. Related questions were discussed in the context of “partial algebraization” of the spectrum [19, 20].

In a closely related development, it was found [21, 22] that it was possible to engineer quantum chaotic Hamiltonians so that specific eigenstates violate the eigenstate thermalization hypothesis (ETH) and therefore could also be considered as quantum scars. Indeed, one of the main theoretical motivations to study many-body scars was concerning the conditions for the violation of the ETH and more generally with the process of thermalization in closed quantum many-body systems.

Another major interest in quantum scars comes from quantum information applications [23, 24]. Thermalization, which is generic in many-body quantum chaotic systems is fast which makes it difficult to use them for encoding and manipulating quantum information. Many-body localized systems do not suffer from this problem, but their low entanglement is a serious drawback for quantum information applications that typically require ample entanglement resources. In principle, it is plausible to expect that quantum scars are also configurations with low entanglement. However, it has been shown that this

* amgg@sjtu.edu.cn

† zhongling_lu@sjtu.edu.cn

‡ ld710@cam.ac.uk

§ jacobus.verbaarschot@stonybrook.edu

is not always the case. The so-called *rainbow scars* [25–27] can have an entanglement entropy that satisfies a volume law [26]. More interestingly, the level of entanglement can be modified [27], at least to some extent, by tuning the parameters of the model; see Ref. [28] for a recent review.

So far the discussion has been restricted to Hermitian systems. However, in the aforementioned quantum information setting, the unavoidable measuring protocol makes the dynamics effectively non-Hermitian. The same applies if we consider the effect of an environment which is described by a similar formalism [29]. Therefore, a natural and rather fundamental problem to investigate is the existence and characteristics of quantum scars in this more general setting.

The literature [24, 30–33] on this problem is still rather scarce. The skin-effect [31] has been employed to identify a scarred eigenstate in a non-Hermitian projected spin model. The same model was used [30] to characterize non-Hermitian scars as states with low entanglement entropy and leading to revivals. The steady state of a vectorized Lindbladian at finite temperature, a thermofield double state, has been characterized as a many-body scar [34]. Finally, very recently, Refs. [35, 36] reported the existence of revivals due to many-body scars in a Lindblad setting. However, even basic questions like the characterization of many-body scars in dissipative quantum systems and their entanglement features are still poorly understood.

The main goal of this paper is to address the above questions by providing a detailed description of scars in vectorized Liouvillians that describe the dynamics of many-body quantum chaotic systems coupled to a Markovian bath. This would open new research avenues in dissipative quantum chaos where even basic questions such as its very definition [37] or the precise role and meaning of the ETH [38–42] are still being debated. In the context of quantum information, it would allow for a more precise assessment of the potential of quantum scars as entanglement resources once the unavoidable process of measurement is taken into consideration.

For these purposes, we shall employ the so-called Lindbladian Sachdev-Ye-Kitaev (SYK) model [43–48] that describes the dynamics of an SYK model [49–56] in contact with a Markovian bath. The SYK model is zero-dimensional, which makes it possible to reach larger sizes while keeping [56–58] all distinct features of many-body quantum chaos. Moreover, it is a toy model for holography [55, 56]; in a certain region of parameters, our results may thus have a gravity dual interpretation. We shall see explicitly that the main results of the paper are not specific to the SYK model but also apply to other strongly interacting systems such as spin models. We start with the definition and general discussion of scar states.

II. VECTORIZED LINDBLADIAN AND MANY-BODY SCARS

We explore the existence and characterization of many-body scars in quantum chaotic systems coupled to a Markovian bath. The time evolution of the density matrix of the system $\hat{\rho}$ is governed by a Liouvillian \mathcal{L} of Lindblad form [59, 60],

$$\partial_t \hat{\rho} = \mathcal{L}(\hat{\rho}) = -i[\hat{H}, \hat{\rho}] + \mu \sum_{\alpha} \left(\hat{L}_{\alpha} \hat{\rho} \hat{L}_{\alpha}^{\dagger} - \frac{1}{2} \{ \hat{L}_{\alpha}^{\dagger} \hat{L}_{\alpha}, \hat{\rho} \} \right), \quad (1)$$

where \hat{H} is the many-body quantum chaotic Hamiltonian and \hat{L}_{α} are the jump operators that characterize coupling to the bath with strength μ . In order to study the evolution of the density matrix, we follow the standard procedure [61] of writing the rows of the matrix as successive columns. This is known as the operator-state mapping, i.e. an operator \hat{O} in the original Hilbert space \mathcal{H} is mapped to a state $|\mathcal{O}\rangle$ in a doubled Hilbert space $\mathcal{H}_2 = \mathcal{H} \otimes \mathcal{H}^* \equiv \mathcal{H}^L \otimes \mathcal{H}^R$, where $*$ stands for the dual space. The resulting Liouvillian, usually referred to as the vectorized Liouvillian, is given by

$$\mathcal{L} = -iH_0 + H_I, \quad (2)$$

where $H_0 = H^L - H^R$ and H_I represents the dissipative term. H^L and H^R can also be interpreted as the Hamiltonian on the backward and forward Keldysh contours, respectively. For specific choices of \hat{H} , such as a SYK model, this general construction may be dual [62] to a weakly perturbed global de-Sitter geometry in two dimensions, which might be unstable towards the formation of Keldysh wormholes [63]. The precise form of H^L , H^R , and H_I depends on the choice of the mapping (i.e., vectorization). We discuss different possibilities below, which we show to correspond to distinct basis choices for the doubled Hilbert space.

A Hamiltonian analogue of Eq. (2) with $iH^L \rightarrow H^L$, $-iH^R \rightarrow H^R$, and H_I Hermitian, was introduced [26, 27] to construct so-called *rainbow scars* [25]. Similarly, many-body scars can also be constructed for the Liouvillian \mathcal{L} Eq. (2) as follows. The thermofield double state (TFD) at infinite temperature [64],

$$|0\rangle = \frac{1}{D} \sum_{i=1}^D |s_i^L\rangle |s_i^R\rangle, \quad (3)$$

where $|s_i^L\rangle$ ($|s_i^R\rangle$) are the eigenstates of H^L (H^R) and D is the Hilbert space dimension, is an eigenstate¹ of $H_0 =$

¹ The term ‘eigenstate’ is used throughout this work to refer to the eigenmodes of the vectorized Liouvillian. They are equivalently

$H^L - H^R$ with eigenvalue zero due to the relative minus sign between H^L and H^R . Contrary to the Hermitian setting of Ref. [26], where one needs to introduce the relative sign by hand, here it is inherent to the Lindblad formalism that describes a single system coupled to a bath.

If the TFD is also an eigenstate of the interacting part H_I , then it becomes an eigenstate of the whole Liouvillian. The TFD corresponds to the vectorization of the identity matrix and hence it is an eigenstate of H_I with real eigenvalue $\mu\lambda$ if $\sum_\alpha [\widehat{L}_\alpha, \widehat{L}_\alpha^\dagger] = \lambda\mathbb{1}$. In particular, if $\lambda = 0$, the TFD corresponds to the steady state of the Liouvillian, which always exists in the spectrum.

The above example shows a trivial example of a scar. Inspired by it, we define a *Lindblad* many-body scar as a simultaneous eigenstate of H_0 and H_I in Eq. (2) whose eigenvalue is the same for an entire family of Liouvillians. For example, if the Liouvillian is disordered, the latter restriction guarantees that the eigenvalue of the scar state is independent of the disorder realization. However, in general, the scarred eigenvector will depend on the disorder realization. For concreteness, we will focus only on the case where the scar vanishes under the action of H_0 and hence its eigenvalue is completely determined by the dissipative part H_I . The same definition can be formulated in the original operator language of the Lindblad equation. Let $\widehat{\mathcal{O}}$ be the operator that corresponds to the vectorized state $|\mathcal{O}\rangle$. $|\mathcal{O}\rangle$ is a scar if $\widehat{\mathcal{O}}$ satisfies the following two conditions:

- (i) $[\widehat{H}, \widehat{\mathcal{O}}] = 0$,
- (ii) $\sum_\alpha \left(\widehat{L}_\alpha \widehat{\mathcal{O}} \widehat{L}_\alpha^\dagger - \frac{1}{2} \left\{ \widehat{L}_\alpha^\dagger \widehat{L}_\alpha, \widehat{\mathcal{O}} \right\} \right) = \eta \widehat{\mathcal{O}}$,

where η is a constant. We thus have that $\mathcal{L}[\widehat{\mathcal{O}}] = \mu\eta\widehat{\mathcal{O}}$. In the remainder of the paper, we will restrict our attention to Hermitian jump operators, $\widehat{L}_\alpha = \widehat{L}_\alpha^\dagger$ that satisfy $\widehat{L}_\alpha^2 = a\mathbb{1}$ with constant a , in which case H_I is Hermitian and the TFD becomes the steady state. In this case, condition (ii) simplifies to

$$(ii') \sum_\alpha \widehat{L}_\alpha \widehat{\mathcal{O}} \widehat{L}_\alpha = \eta' \widehat{\mathcal{O}},$$

for some real constant η' related to η by a shift.

The main feature of the scar states is that their eigenvalues can be obtained analytically and do not depend on the details of \widehat{H} . To see this, first note that for *any* matrix, the real and imaginary part of the eigenvalues are related to expectation values of the Hermitian and anti-Hermitian parts of the matrix. Indeed, for an eigenstate $|k\rangle$, let $\mathcal{L}|k\rangle = \lambda_k|k\rangle$, where $\mathcal{L} = -iH_0 + H_I$ is decomposed into its Hermitian part H_I and anti-Hermitian part $-iH_0$ and $\lambda_k = a_k + ib_k$ with $a_k, b_k \in \mathbb{R}$. Then, this leads

to $-i\langle k|H_0|k\rangle + \langle k|H_I|k\rangle = a_k + ib_k$, and because a_k and b_k are real and H_0 and H_I are Hermitian, it follows that $a_k = \langle k|H_I|k\rangle$, $b_k = -\langle k|H_0|k\rangle$. This is not helpful for generic eigenstates of the Liouvillian. However, scar states are also eigenstates of H_0 and H_I individually, and therefore, the eigenvalues of scar states can be obtained without diagonalization. In particular, because of condition (i), we have $b_k = 0$, and by condition (ii'), $a_k = \mu\eta$ for any choices of H_0 consistent with condition (i). In Sec. IV, we will see that this construction relates to the operator size in open quantum systems.

As an illustration of the above analysis, we now identify many-body scars in a SYK model coupled to a Markovian bath for both Majorana and complex fermions.

III. LINDBLAD SCARS IN THE SYK MODEL

A. Dissipative Majorana SYK model

We first investigate the Lindbladian Majorana SYK model [43–48] described by the Liouvillian Eq. (1) with

$$\widehat{H} = -i^{\frac{q}{2}} \sum_{1 \leq i_1 < i_2 < \dots < i_q \leq N} K_{i_1 i_2 \dots i_q} \psi_{i_1} \psi_{i_2} \dots \psi_{i_q} \quad (4)$$

where ψ_i are Majorana fermions, $\{\psi_i, \psi_j\} = \delta_{ij}$, $K_{i_1 i_2 \dots i_q}$ are Gaussian random couplings with zero mean and variance $2^{q-1}(q-1)!N^{1-q}/q$, N is even and q is an even integer. The Markovian bath enters in the Lindblad equation through the jumps operators, which we choose as $\widehat{L}_i = \psi_i$. Because $\widehat{L}_i^\dagger \widehat{L}_i = \mathbb{1}/2$, the term $\{\sum_\alpha \widehat{L}_\alpha^\dagger \widehat{L}_\alpha, \widehat{\rho}\}$ is simply an overall shift of the Lindbladian.

The vectorization of the Liouvillian is not unique. While different vectorization schemes correspond to unitary transformations of the Liouvillian and therefore leave, e.g., the spectrum invariant, they give rise to different partitions of the many-body Hilbert space and, therefore, affect quantities that are sensitive to them such as the size discussed in Sec. IV and the entanglement entropy discussed in Sec. V. We start this section by precisely discussing different choices of vectorization.

A commonly used [45] set of left and right Majorana fermions is given by

$$\chi_k^L = \psi_k \otimes \mathbb{1}, \quad \chi_k^R = \widehat{P} \otimes \psi_k, \quad (5)$$

where the parity operator $\widehat{P} = 2^{N/2} i^{N(N-1)/2} \prod_{k=1}^N \psi_k$ anti-commutes with all ψ_k (i.e., \widehat{P} is the Γ_5 matrix for the Euclidean N -dimensional gamma matrices that represent the fermions). With this representation, the left, right,

eigenoperators of the Lindblad equation in the original Hilbert space due to the operator-state mapping.

and interaction terms in the Liouvillian read [45]:

$$H^L = -i^{\frac{q}{2}} \sum_{1 \leq i_1 < \dots < i_q \leq N} K_{i_1 i_2 \dots i_q} \chi_{i_1}^L \dots \chi_{i_q}^L, \quad (6)$$

$$H^R = -i^{\frac{q}{2}} (-1)^{q/2} \sum_{1 \leq i_1 < \dots < i_q \leq N} K_{i_1 i_2 \dots i_q} \chi_{i_1}^R \dots \chi_{i_q}^R, \quad (7)$$

$$H_I = i\mu \sum_i \chi_i^L \chi_i^R - \frac{N\mu}{2}. \quad (8)$$

We can construct a different set of Majoranas by the unitary transformation

$$U = e^{i\pi \hat{P}/4} \otimes \hat{C}, \quad (9)$$

with \hat{C} the unitary charge conjugation matrix satisfying $\hat{C}\psi_k\hat{C}^{-1} = \psi_k^*$. This gives the Majorana fermions

$$\tilde{\chi}_k^L = U\chi_k^L U^{-1} = i\hat{P}\psi_k \otimes \mathbb{1}, \quad (10)$$

$$\tilde{\chi}_k^R = U\chi_k^R U^{-1} = \hat{P} \otimes \psi_k^*. \quad (11)$$

The left-right coupling can be rewritten as

$$\begin{aligned} U i \chi_k^L \chi_k^R U^{-1} &= -(\hat{P}\psi_k \otimes \mathbb{1})(\hat{P} \otimes \psi_k^*) \\ &= (\psi_k \otimes \mathbb{1})(\mathbb{1} \otimes \psi_k^*) \equiv \tilde{\chi}_k^L \tilde{\chi}_k^R, \end{aligned} \quad (12)$$

where we have introduced the ‘‘pseudo-fermions’’

$$\tilde{\chi}_k^L = \psi_k \otimes \mathbb{1}, \quad \tilde{\chi}_k^R = \mathbb{1} \otimes \psi_k^*. \quad (13)$$

These left and right fermions anti-commute among themselves, but all left fermions commute with all right fermions. However, this not problematic because the Liouvillians in the two representations are related by a unitary transformation. The interaction H_I thus reads

$$H_I = \mu \sum_{k=1}^N \tilde{\chi}_k^L \tilde{\chi}_k^R - \frac{N\mu}{2}. \quad (14)$$

It is clear that H^L and H^R can also be rewritten in terms of these pseudo-fermions:

$$\sum_{i_1 \leq \dots \leq i_q} \chi_{i_1}^L \dots \chi_{i_q}^L = \sum_{i_1 \leq \dots \leq i_q} \tilde{\chi}_{i_1}^L \dots \tilde{\chi}_{i_q}^L \quad (15)$$

$$(-1)^{\frac{q}{2}} \sum_{i_1 \leq \dots \leq i_q} \chi_{i_1}^R \dots \chi_{i_q}^R = \sum_{i_1 \leq \dots \leq i_q} \tilde{\chi}_{i_1}^R \dots \tilde{\chi}_{i_q}^R. \quad (16)$$

All vectorization schemes give the same results for quantities that are basis invariant, such as the spectrum. However, as we will see in Sec. V, it is advantageous to use these pseudo-fermions for the calculation of the entanglement entropy.

The SYK Hamiltonian commutes only with the parity operator (and trivially with itself) and hence $\hat{O} = \hat{H}, \hat{P}$, and $\hat{H}\hat{P}$ satisfy the scar condition (i). Moreover, they

also satisfy condition (ii’):

$$\sum_{\alpha} \psi_{\alpha} \hat{P} \psi_{\alpha} = -\frac{N}{2} \hat{P}, \quad (17)$$

$$\sum_{\alpha} \psi_{\alpha} \hat{H} \psi_{\alpha} = \left(\frac{N}{2} - q\right) \hat{H}, \quad (18)$$

$$\sum_{\alpha} \psi_{\alpha} \hat{H} \hat{P} \psi_{\alpha} = -\left(\frac{N}{2} - q\right) \hat{H} \hat{P}. \quad (19)$$

This allows the construction of three more scar states in addition to the identity operator: \hat{P} , \hat{H} , and $\hat{P}\hat{H}$, with eigenvalues $-N\mu$, $-q\mu$, and $-(N-q)\mu$, respectively.

The same calculation can be done in the vectorized model. For instance, the parity operator is mapped to the left parity, $P^L = 2^{N/2} i^{N(N-1)/2} \prod_{k=1}^N \chi_k^L$, acting on the TFD $|0\rangle$. Then,

$$\begin{aligned} i \sum_k \chi_k^L \chi_k^R P^L |0\rangle &= i \sum_k \chi_k^L P^L \chi_k^R |0\rangle \\ &= \sum_k \chi_k^L P^L \chi_k^L |0\rangle = -\frac{N}{2} P^L |0\rangle, \end{aligned} \quad (20)$$

where in the second step we have used operator reflection [45]. Taking into account the constant term of the vectorized operator, we find a scar state with eigenvalue $-\mu N$. The second scar, $\hat{O} = \hat{H}$, can be implemented in a similar fashion for the vectorized operator:

$$\begin{aligned} i \sum_k \chi_k^L \chi_k^R H^L |0\rangle &= i \sum_k \chi_k^L H^L \chi_k^R |0\rangle \\ &= \sum_k \chi_k^L H^L \chi_k^L |0\rangle = \left(\frac{N}{2} - q\right) H^L |0\rangle. \end{aligned} \quad (21)$$

Taking into account the constant term in the vectorized Liouvillian, this gives a scar state with eigenvalue $-q\mu$. Similarly, the last symmetry gives an eigenstate with eigenvalue $-(N-q)\mu$. We thus have found four scar states:

$$|0\rangle, \quad P^L |0\rangle, \quad H^L |0\rangle, \quad H^L P^L |0\rangle. \quad (22)$$

Note that $(H^L)^2$ and higher powers of H^L do not satisfy the symmetry relations (ii’). Therefore, there are no additional scars in the dissipative Majorana SYK model.

To numerically confirm the analytical results, we computed the spectrum of the dissipative Majorana SYK model with linear jump operators for $N = 12$ and $\mu = 0.1$, see Fig. 1 (left). The eigenvalues of the scar states are denoted by red crosses and blue circles and occur at the locations explained before.

B. Dissipative complex SYK model

To find a richer structure of scar states, we consider the complex SYK Hamiltonian with $U(1)$ symmetry. To this

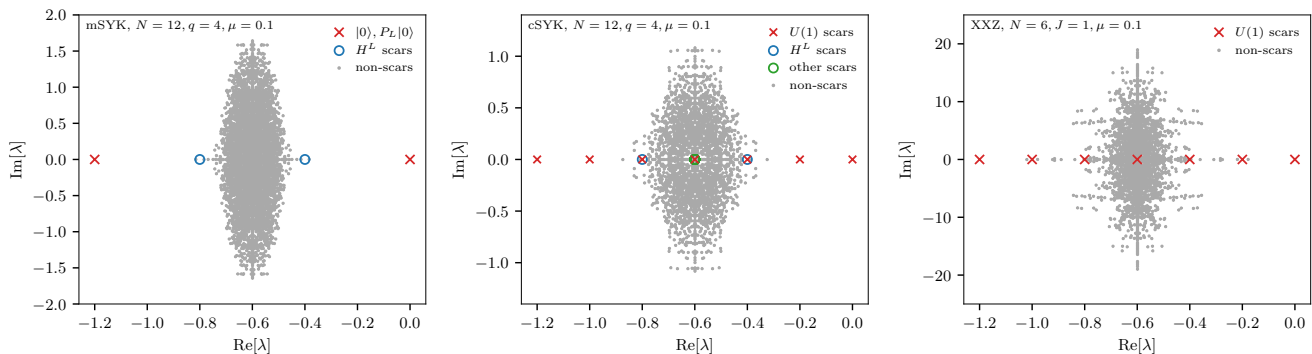


Figure 1. Spectrum λ of one realization of the SYK Liouvillian with linear jump operators, with $q = 4$ and $N = 12$, (left and middle) and of the XXZ spin model (right). Non-scar states are denoted by grey dots. Left: Majorana SYK Hamiltonian Eq. (4), which has two parity (red crosses) and two H^L scars (blue circles). Middle: complex SYK Hamiltonian Eq. (26), which displays $N/2 + 1$ $U(1)$ scars (red crosses) and two H^L scars (blue circles), which are fully characterized in the text, as well as fourteen degenerate “other scars” (green circles) for which we could not find a full characterization. Right: the XXZ model (52) with weak dissipation (note the scale of the y -axis). In this case we only found the $U(1)$ scars. All scar eigenvalues have zero imaginary part and an analytically determined real part that does not depend on the disorder realization of the Hamiltonian.

end, we introduce the projection operator into a sector of fixed charge (i.e., particle number) n ,

$$\hat{\mathbb{P}}_n = \hat{\mathbb{P}}_n^2 = \hat{\mathbb{P}}_n^\dagger. \quad (23)$$

Explicitly, let us consider complex fermions $a_i = (\psi_{2i-1} - i\psi_{2i})/\sqrt{2}$, whose number operator

$$\hat{\mathcal{N}} = \sum_{i=1}^{N/2} a_i^\dagger a_i = \sum_{i=1}^{N/2} \left(\frac{1}{2} - i\psi_{2i-1}\psi_{2i} \right) \quad (24)$$

has eigenvalues $n = 0, \dots, N/2$. The projection operator onto the sector with charge n is given by

$$\hat{\mathbb{P}}_n = \frac{1}{N/2 + 1} \sum_{s=0}^{N/2} \exp \left\{ \frac{2\pi i s}{N/2 + 1} (\hat{\mathcal{N}} - n) \right\} \quad (25)$$

and the complex SYK model is then obtained by summing over the projection onto all sectors,

$$\hat{H}_c = \sum_{n=0}^{N/2} \hat{\mathbb{P}}_n \hat{H} \hat{\mathbb{P}}_n. \quad (26)$$

In a representation where the number operator is diagonal, we conjecture that this Hamiltonian agrees with the antisymmetrized complex SYK Hamiltonian introduced in Ref. [65]. This can be shown analytically for $q = 2$, while for $q = 4$, we only have numerical evidence. The jump operators are chosen the same as in the Majorana case, namely, $\hat{L}_i = \psi_i$. It is crucial that the jump operators do not respect the $U(1)$ symmetry. If they did, the whole Liouvillian would have a strong [66] $U(1)$ symmetry and the symmetry operator would lead to block diagonalization of \mathcal{L} instead of inducing a scar.

If the number operator of the k -th complex fermion is given by

$$\hat{n}_k = a_k^\dagger a_k = \frac{1}{2} - i\psi_{2k-1}\psi_{2k}, \quad (27)$$

then we define the p -tuple operator as

$$\hat{\mathcal{N}}_p = \sum_{k_1 \neq k_2 \neq \dots \neq k_p} \left(\hat{n}_{k_1} - \frac{1}{2} \right) \left(\hat{n}_{k_2} - \frac{1}{2} \right) \dots \left(\hat{n}_{k_p} - \frac{1}{2} \right). \quad (28)$$

These operators commute with \hat{H}_c [condition (i)] and are acted on by the jump operators as [condition (ii)]

$$\sum_k \psi_k \hat{\mathcal{N}}_p \psi_k = \left(\frac{N}{2} - 2p \right) \hat{\mathcal{N}}_p, \quad (29)$$

where p takes the values, $0, 1, \dots, N/2$, resulting in $N/2 + 1$ scar states with eigenvalue $-2p\mu$. For the vectorized Liouvillian, they are given by

$$\mathcal{L} \mathcal{N}_p^L |0\rangle = -2p\mu \mathcal{N}_p^L |0\rangle. \quad (30)$$

Then the $U(1)$ scar states of the vectorized Liouvillian are given by $\mathcal{N}_p^L |0\rangle$. We note that the p -tuple operators can be expressed as linear combinations of powers of the number operator,

$$\hat{\mathcal{N}}_p = \sum_{k=0}^p c_{pk} \hat{\mathcal{N}}^k, \quad (31)$$

with c_{pk} combinatorial factors that can be calculated recursively. Indeed, the operators $\hat{\mathcal{N}}_p$ defined in (28) satisfy

the relation

$$\widehat{\mathcal{N}}_{p+1} = \left(\widehat{\mathcal{N}} - \frac{N}{2} \right) \widehat{\mathcal{N}}_p - \frac{p}{4} (N - p + 1) \widehat{\mathcal{N}}_{p-1}, \quad (32)$$

with initial conditions $\widehat{\mathcal{N}}_0 = \mathbb{1}$ and $\widehat{\mathcal{N}}_1 = \widehat{\mathcal{N}} - N/2$. For \mathcal{N}_2 and \mathcal{N}_3 we obtain

$$\widehat{\mathcal{N}}_2 = \left(\widehat{\mathcal{N}} - \frac{N}{2} \right)^2 - \frac{N}{4}, \quad (33)$$

$$\widehat{\mathcal{N}}_3 = \left(\widehat{\mathcal{N}} - \frac{N}{2} \right)^3 - \left(\frac{3}{4}N - \frac{1}{2} \right) \left(\widehat{\mathcal{N}} - \frac{N}{2} \right). \quad (34)$$

As was the case for Majorana fermions, there is an additional scar state at both $-q\mu$ and $-(N-q)\mu$, which are given by

$$H_c^L|0\rangle, \quad H_c^L P^L|0\rangle, \quad (35)$$

respectively. The existence of these scars still follows from Eqs. (18) and (19). Indeed, the projectors $\widehat{\mathbb{P}}_n$ discard non-charge conserving terms from H but do not change the number q of Majorana operators in each term in \widehat{H}_c . Therefore, the commutation relation with H_I is left unchanged and these scars also exist in the $U(1)$ conserving system.

Are these the only scar eigenstates of the Lindbladian complex SYK model? We performed numerical checks for $N = 12$, and selected the scar states by the requirement that they are joint eigenstates of $H^L - H^R$ and H_I . To obtain disorder-independent eigenvalues, they must be eigenstates of $H^L - H^R$ with eigenvalue zero, so a necessary requirement is that the eigenvalues of \mathcal{L} are equal to $\{-N\mu, (-N+2)\mu, \dots, 0\}$. When these states are non-degenerate, they are also eigenstates of H_I and are scar states with the same eigenvalue. When they are degenerate, a complication arises since they can be linear combinations of scar and non-scar states. In order to disentangle the scar and non-scar states, we determine the singular values of $\langle \alpha | H_I - 2k\mu | 2k \rangle$, with $|2k\rangle$ the eigenstates of \mathcal{L} with eigenvalue $2k\mu$ and $|\alpha\rangle$ a complete set of states. Only the states corresponding to singular value zero are scar states. Following this procedure, we find a single scar eigenstate for all $-2p\mu$ except for $-q\mu$, $-(N-q)\mu$, and $-N\mu/2$. At $-q\mu$, there are two scar eigenstates given by $\mathcal{N}_1^L|0\rangle$ and $\widehat{H}_c^L|0\rangle$ as discussed above. The same applies for the two scars at $-(N-q)\mu$. However, we find an N -dependent number of additional scars in the middle of the spectrum, i.e., at $-N\mu/2$. For $N = 12$, we find fifteen scar states at zero, and for $N = 16$ there are nineteen scars also at zero, and both numbers include one $U(1)$ scar. Because of the degeneracy they cannot be separated from the $U(1)$ scar state. As an example, we present in Fig. 1 (middle) a scatter plot of the eigenvalues of the complex SYK model Eq. (26) with linear jump operators for $N = 12$ and $\mu = 0.1$.

IV. CHARACTERIZATION OF LINDBLAD SCARS BY OPERATOR SIZE

So far we have not analyzed the properties of the eigenstates of scar states, which we expect to behave qualitatively differently from the surrounding quantum chaotic eigenstates. In this section, we address this issue by showing that the operator size, which is a popular indicator of quantum chaos, provides a sharp distinction between the Lindblad scars introduced earlier and the rest of eigenstates, which in the SYK model, are expected to be quantum chaotic.

In a fermionic system, the operator size is a measure of the (average) number of Majorana operators in an expansion of the operator in the basis of Majorana strings. A Majorana string of size p is given by

$$\Gamma_{\underline{n}} = 2^{p/2} \psi_{n_1} \cdots \psi_{n_p}, \quad (36)$$

with $n_1 \leq n_2 \leq \dots \leq n_p$. It satisfies the orthogonality relation $\text{Tr} [\Gamma_{\underline{n}} \Gamma_{\underline{m}}] = \delta_{\underline{n}\underline{m}}$. Hence, the set of all 2^N possible strings forms a basis of the space of operators on the Hilbert space \mathcal{H}_1 and any operator can be expressed as a linear combination of these basis operators. The size operator \mathcal{S} can be defined as

$$\mathcal{S}(\widehat{\mathcal{O}}) = \sum_{k=1}^N [\widehat{\mathcal{O}}, \psi_k]_{\pm} \psi_k = \frac{N}{2} \widehat{\mathcal{O}} \pm \sum_{k=1}^N \psi_k \widehat{\mathcal{O}} \psi_k, \quad (37)$$

where we choose the anti-commutator when the number of fermions in \mathcal{O} is odd. We immediately see that the vectorized \mathcal{S} ,

$$\mathcal{S} = \frac{N}{2} - i \sum_i \chi_i^L \chi_i^R, \quad (38)$$

satisfies $\mathcal{S} = -H_I/\mu$ for H_I given by Eq. (6) with our choice of jump operators, $L_i = \psi_i$. Hence, it follows that condition (ii) is equivalent to $\widehat{\mathcal{O}}$ being an eigenstate of the size superoperator. More precisely, we have that

$$\mathcal{S}(\Gamma_{\underline{n}}) = p \Gamma_{\underline{n}}, \quad (39)$$

i.e., the Majorana strings are the eigenvectors of the size superoperator with eigenvalue p (the length of vector \underline{n}).

A generic operator $\widehat{\mathcal{O}}$ is not an eigenstate of the size operator. In this case, we can define its size as

$$\langle \mathcal{S} \rangle_{\widehat{\mathcal{O}}} = \frac{\text{Tr} [\widehat{\mathcal{O}}^\dagger \mathcal{S}(\widehat{\mathcal{O}})]}{\text{Tr} [\widehat{\mathcal{O}}^\dagger \widehat{\mathcal{O}}]}. \quad (40)$$

Denoting the normalized right eigenstates of the vectorized Liouvillian by $|\alpha\rangle$, the size of this state is given

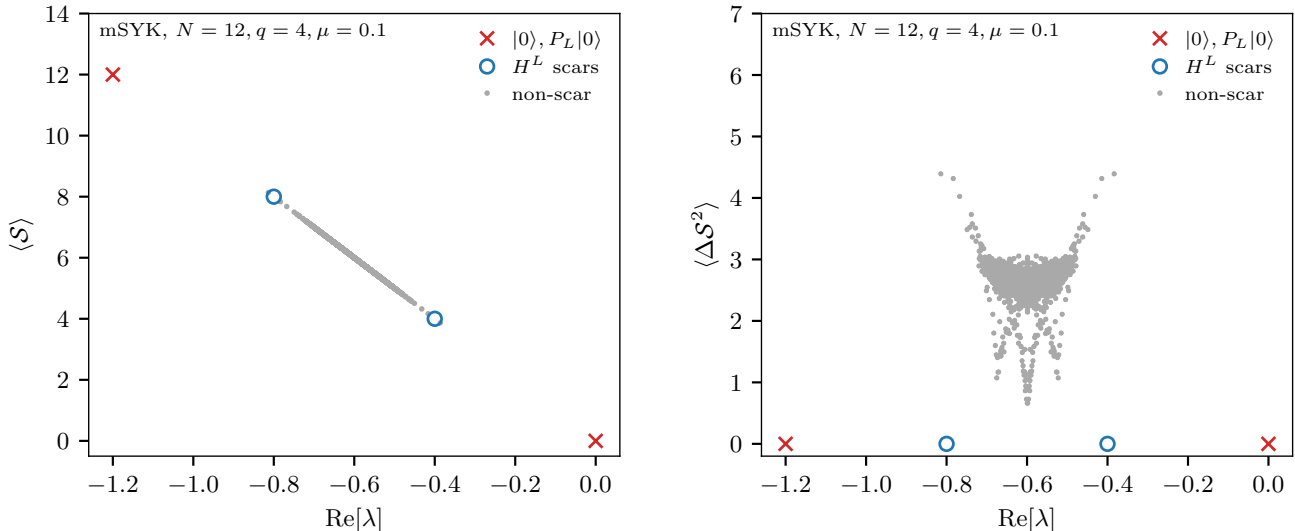


Figure 2. Operator size Eq. (38) of the eigenstates for one realization of the vectorized Liouvillian of the Majorana SYK model Eq. (4) for $N = 12$, $q = 4$, and $\mu = 0.1$ as a function of the real part of the eigenvalues $\text{Re}[\lambda]$. Scar states are denoted by red crosses and blue circles and non-scar states by grey dots. Left: Operator size average, Eq. (41). There is a simple linear relation between the size of the eigenstates and the real part of the corresponding eigenvalues, as expected. Right: Operator size variance, $\Delta \mathcal{S}^2 = \langle \mathcal{S}^2 \rangle - \langle \mathcal{S} \rangle^2$. Only the scar states have a distinct vanishing variance since they are shared eigenstates of the Liouvillian and the size operator.

by

$$\langle \mathcal{S} \rangle = N/2 - \sum_{i=1}^N \langle \alpha | \chi_i^L \chi_i^R | \alpha \rangle. \quad (41)$$

Here and below we use the notation $\langle \cdot \rangle$ for the expectation value $\langle \alpha | \cdot | \alpha \rangle$ of state $|\alpha\rangle$.

In Fig. 2, we depict results for the average and variance of the size Eq. (41) for the Liouvillian of the $q = 4$ SYK Hamiltonian Eq. (26) with linear jump operators and $\mu = 0.1$. Since the real part of the eigenvalues λ of \mathcal{L} is equal to the expectation value of H_I we find that the size is a linear function of $\text{Re}[\lambda]$, see Fig. 2 (left). Therefore, the size cannot be used to distinguish scar from non-scar states. However, since scars are shared eigenstates of the Liouvillian and the size operator, the variance of the scar states vanishes, while for the non-scar states it is positive (see Fig. 2, right), and can thus be used to distinguish scar states from non-scar states. Their number agrees with the discussion in Sec. II.

In order to characterize scar states further, we can eliminate the reliance of the operator size on the real part of the eigenvalues by separating the size contribution into different parts, e.g., odd and even Majoranas.

Specifically, in the complex SYK model, we define

$$\mathcal{S}_o = \frac{N}{4} - i \sum_{i=1}^{N/2} \chi_{2i-1}^L \chi_{2i-1}^R, \quad (42)$$

$$\mathcal{S}_e = \frac{N}{4} - i \sum_{i=1}^{N/2} \chi_{2i}^L \chi_{2i}^R. \quad (43)$$

To eliminate the dependence on the total size, we will focus on the observable $\mathcal{S}_e - \mathcal{S}_o$ in the rest of the section. We consider the expectation values

$$\langle \mathcal{S}_e - \mathcal{S}_o \rangle \quad (44)$$

and

$$\langle (\mathcal{S}_e - \mathcal{S}_o)^2 \rangle. \quad (45)$$

In the Majorana SYK case, see Fig. 3, we observe that the average and the second moment of $\mathcal{S}_e - \mathcal{S}_o$ are qualitatively different for scars and non-scar states. Moreover, the TFD scar $|0\rangle$ is the fermionic vacuum and hence has the same number of even and odd Majoranas, namely, zero. Likewise, the scar $P^L|0\rangle$ is the completely-filled state and has the maximal number $N/2$ of even and odd Majoranas. Accordingly, both scars are eigenstates of both \mathcal{S}_e and \mathcal{S}_o with the same eigenvalue and the expectation values in Eqs. (44) and (45) vanish. On the other hand, H^L is a sum of terms that do not have a fixed number of even (or odd) Majoranas; indeed, there are terms with $0, 1, \dots, q$ even (or odd) Majoranas. Therefore, the

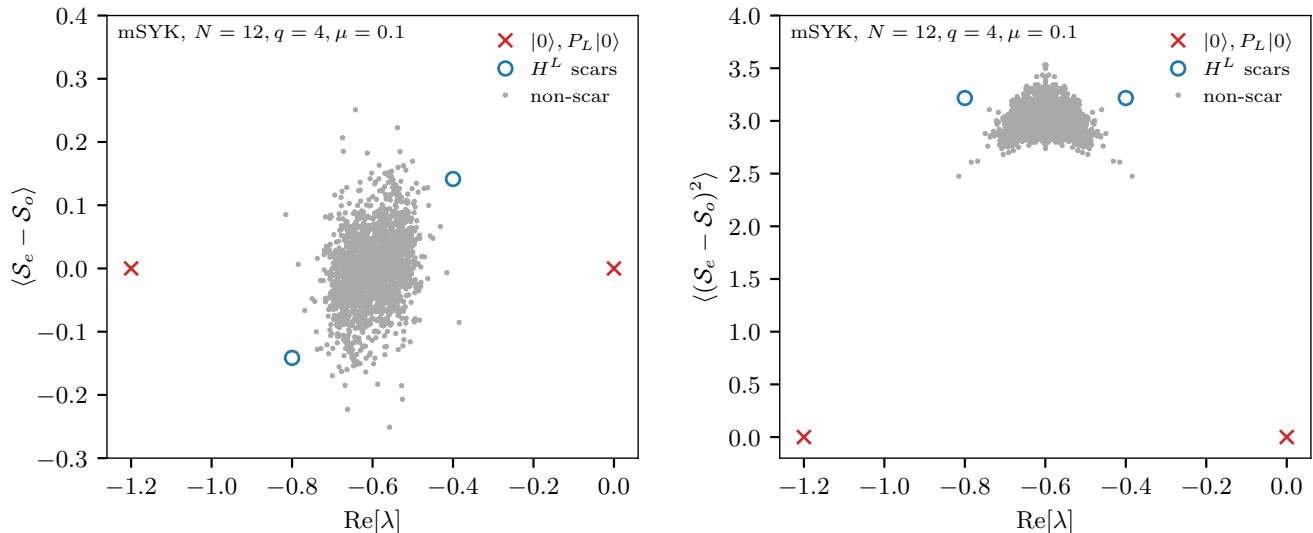


Figure 3. Expectation values of $\mathcal{S}_e - \mathcal{S}_o$, Eq. (44) (left), and $(\mathcal{S}_e - \mathcal{S}_o)^2$, Eq. (45) (right), for one realization of the vectorized Liouvillian of the Majorana SYK model Eq. (4) for $N = 12$, $q = 4$, and $\mu = 0.1$ as a function of the real part of the eigenvalues $\text{Re}[\lambda]$. Scar states are denoted by red crosses and blue circles and non-scar states by grey dots. Only the parity scars have vanishing moments of $\mathcal{S}_e - \mathcal{S}_o$ because they are simultaneous eigenvalues of \mathcal{S}_e and \mathcal{S}_o .

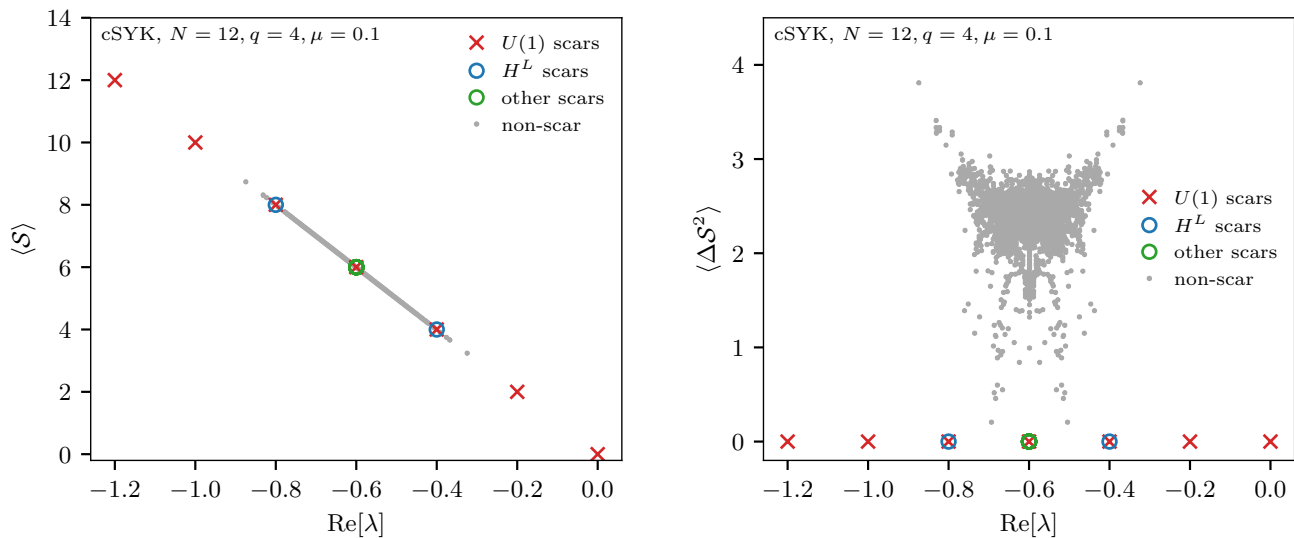


Figure 4. Operator size Eq. (38) of the eigenstates of one realization of the vectorized Liouvillian of the complex SYK model Eq. (26) for $N = 12$, $q = 4$, and $\mu = 0.1$ as a function of the real part of the eigenvalues $\text{Re}[\lambda]$. Scar states are denoted by red crosses and blue and green circles and non-scar states by grey dots. Left: Operator size average, Eq. (41). Right: Operator size variance, $\Delta \mathcal{S}^2 = \langle \mathcal{S}^2 \rangle - \langle \mathcal{S} \rangle^2$. As in the Majorana case, see Fig. 2, the mean of the size depends linearly on $\text{Re}[\lambda]$ and the variance of the sizes vanishes only for scars states.

two H^L scars are not eigenstates of \mathcal{S}_e and \mathcal{S}_o and the expectation values in Eqs. (44) and (45) are finite.

We now turn to the complex SYK case, Eq. (26). For the sake of completeness, we first study the operator size and variance without separating the size contribution of the different parts. We observe, see Fig. 4, a similar pattern as in the Majorana case, although with a much richer scar spectrum, which will be discussed shortly. The op-

erator size is still linear in the real part of the eigenvalues which make it unsuitable for a general characterization of scars. Likewise, scar states size have zero variance because the Liouvillian and the size operator have common eigenstates. Therefore, from now on, we follow the route of the Majorana fermions, and focus on the more interesting case of computing the size of odd and even fermion separately. We refer to the previous discussion

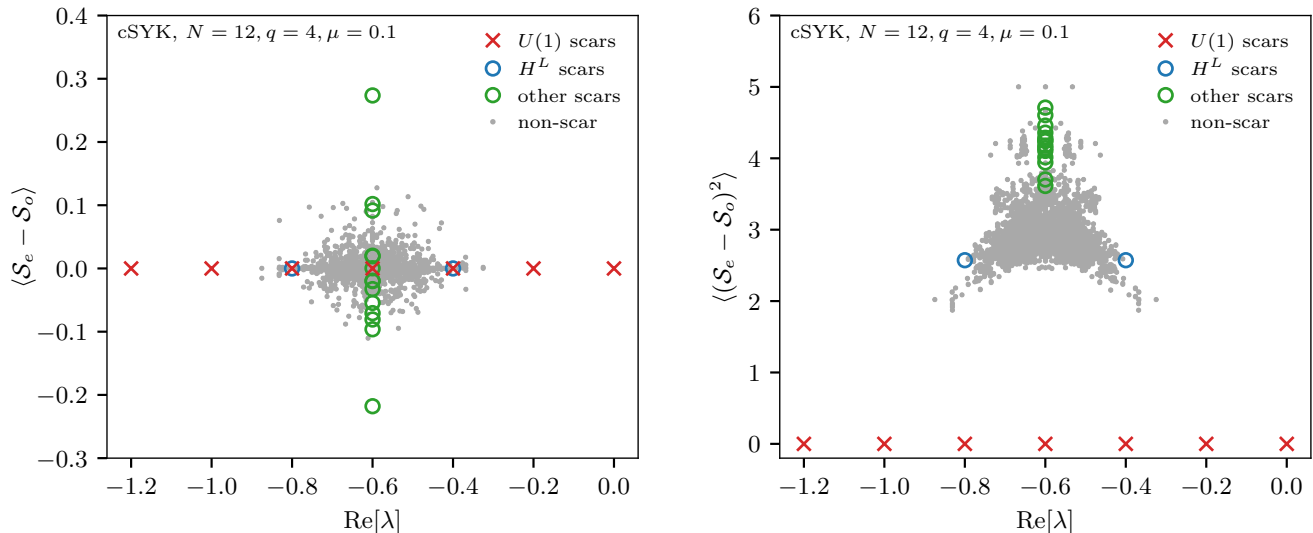


Figure 5. Expectation values of $\mathcal{S}_e - \mathcal{S}_o$, Eq. (44) (left), and $\langle (\mathcal{S}_e - \mathcal{S}_o)^2 \rangle$, Eq. (45) (right), for one realization of the vectorized Liouvillian of the complex SYK model Eq. (26) for $N = 12$, $q = 4$, and $\mu = 0.1$, as a function of the real part of the eigenvalues $\text{Re}[\lambda]$. Scar states are denoted by red crosses and blue and green circles and non-scar states by grey dots. Only the $N/2 + 1$ $U(1)$ scars are simultaneous eigenstates of \mathcal{S}_e and \mathcal{S}_o and hence have vanishing moments of $\mathcal{S}_e - \mathcal{S}_o$.

on Majorana SYK for further details.

The results depicted in Fig. 5 for $\mathcal{S}_e - \mathcal{S}_o$ permit a more detailed study of the richer pattern of many-body scars observed for complex fermions. The predicted $U(1)$ and H^L scars have zero average $\langle \mathcal{S}_e - \mathcal{S}_o \rangle$, Eq. (44), which is the theoretical prediction. Indeed, the $U(1)$ scars are constructed from the operators $\widehat{\mathcal{N}}_p$, Eq. (28), which always have the same number of even and odd Majoranas. Similarly, the projection in \widehat{H}_c ensures² that, when expressed in terms of Majorana fermions, for every term in \widehat{H}_c with a given value of $\mathcal{S}_e - \mathcal{S}_o$, there exists another term with the same coupling but opposite $\mathcal{S}_e - \mathcal{S}_o$, and $\mathcal{S}_e(\widehat{H}_c) - \mathcal{S}_o(\widehat{H}_c)$ vanishes. Moreover, $\widehat{\mathcal{N}}_p$ is a simultaneous eigenstate of both \mathcal{S}_e and \mathcal{S}_o with the same eigenvalue and, hence, also the variance, Eq. (45), vanishes for the $U(1)$ scars. On the other hand, while \widehat{H}_c has $\langle \mathcal{S}_e - \mathcal{S}_o \rangle = 0$ on average, it is not an eigenstate of \mathcal{S}_e and \mathcal{S}_o and therefore the variance is finite.

Surprisingly, we have found fifteen³ scars at $\lambda = -0.6 = -N\mu/2$ that we have labeled as “other scars”. These states are scars because they are eigenstates of $-iH_0$ and H_I with eigenvalue $-N\mu/2$. However, we could not identify to what symmetry of SYK, if any, they are related to. Interestingly, these scars have a varied range of operator size and variance that reinforces the

idea that scars are promising resources for quantum information applications. We note that the analytical $U(1)$ scar at the center of the spectrum is also contained among the “other scars”, and is thus plotted twice. Without a full characterization of these degenerate scars we cannot conclude whether this degeneracy with the $U(1)$ scar is based on symmetry, but there is a possibility that they are connected with a symmetry of the SYK model, or a feature of the jump operators. Therefore, they need not be restricted to this model, although we do not observe them in the XXZ spin chain to be studied in Sec. VI.

Finally, we address the full distribution of the operator size $\langle \mathcal{S}_e - \mathcal{S}_o \rangle$. For states with a nonvanishing expectation value (among others scar states but also many other states) it can be used as a powerful probe of the applicability and relevance of the ETH in many-body quantum dissipative systems. According to the Hermitian ETH [67, 68], we would expect a Gaussian distribution of $\langle \mathcal{S}_e - \mathcal{S}_o \rangle$ with a mean and a width that show a smooth variation as a function of the energy (i.e., an energy dependence on a scale that is much larger than the scale of the fluctuations) [69–72]. For non-Hermitian operators, the spectrum is two-dimensional, and the size operator can have a nontrivial smooth behavior as a function of both the real part and the imaginary part of the eigenvalues. This can be shown by calculating the mean and standard deviation of the nonzero size differences as a function of the eigenvalue using a small bin size and fitting them by smooth functions, $M(\lambda)$ and $\sigma(\lambda)$, in this order. The normalized size difference for a state with

² We can show this explicitly for $q = 2$ and conjecture it to also hold for larger q based on the numerical results.

³ The $U(1)$ scar at the center of the spectrum is completely mixed among these states and cannot be identified separately. However, we can construct it analytically as $\mathcal{N}_{N/4}^L|0\rangle$.

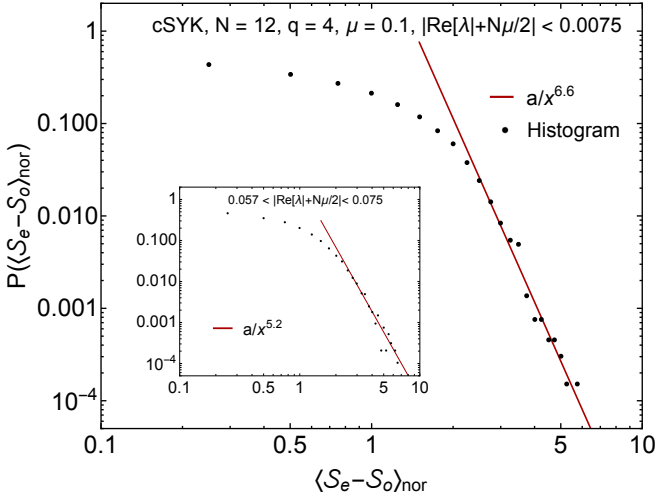


Figure 6. Log-log plot of the histogram of the normalized expectation values $\langle \mathcal{S}_e - \mathcal{S}_o \rangle$ (black points) for the non-scar states of the complex SYK model with $N = 12$, $q = 4$, and $\mu = 0.1$ (for 200 realizations). The distribution is computed for a small window around the center of the spectrum (main) and a window away from the center (inset) with values as indicated in the figure. A fit by the power law a/x^b (red), with the parameters a and b depending on the window of eigenvalues, provides a good description of the asymptotic decay of the distribution. The observed deviations from a Gaussian behavior suggest that ETH in dissipative quantum chaos may be qualitatively different from that in Hermitian quantum chaos [67, 68].

eigenvalue λ is defined by

$$\langle \mathcal{S}_e - \mathcal{S}_o \rangle_{\text{nor}} = \frac{\langle \mathcal{S}_e - \mathcal{S}_o \rangle - M(\lambda)}{\sigma(\lambda)}. \quad (46)$$

As already suggested by Fig. 5 (left), their dependence on the real parts and the imaginary parts of the eigenvalues is relatively weak. After normalization to zero mean and unit variance we can combine results from a group of nearby bins to increase statistics.

After performing this normalization procedure, we find the distribution shown in Fig. 6 (black dots) for $|\text{Re}[\lambda] + N\mu/2| < 0.0075$ (main) and $0.057 < |\text{Re}[\lambda] + N\mu/2| < 0.075$ (inset). In both cases, it has a distinct power-law tail (red curve) with a power that decreases away from the center. Note that on average, the value of $\langle \mathcal{S}_e - \mathcal{S}_o \rangle$ vanishes for about 62% of the states.

While a Gaussian distribution is the broadly accepted expectation for Hermitian systems, the reach and details of the ETH for non-Hermitian systems is still under debate [38–42]. Because the non-stationarity of the normalized distribution of $\langle \mathcal{S}_e - \mathcal{S}_o \rangle_{\text{nor}}$ is negligible for the energy windows for which the distribution was calculated we can exclude this as the cause of the non-Gaussianity. Therefore, these results point to qualitative differences with respect to the Hermitian case that deserve further consideration.

V. CHARACTERIZATION OF LINDBLAD SCARS BY ENTANGLEMENT ENTROPY

The analytical properties and fixed operator sizes of the U(1) scars imply a rather simple operator complexity. A natural conjecture stepped further is that the entanglement entropy of the scars are sub-volume given their simple operator structure. We will see that for Lindblad scars the picture is more complicated because the EE depends sensitively on the choice of the partition. A detailed characterization of the entanglement of the Lindblad scars is important not only for the understanding of the scar itself but also to give insights into quantum many-body effects such as quantum chaos and information scrambling.

The entanglement entropy (EE) of eigenstate $|k\rangle$ of \mathcal{L} is defined as

$$S_{\Omega}^{(k)} = -\text{Tr} \left[\rho_{\Omega}^{(k)} \log \rho_{\Omega}^{(k)} \right], \quad \rho_{\Omega}^{(k)} = \text{Tr}_{\bar{\Omega}} |k\rangle\langle k|, \quad (47)$$

where Ω is a subset of the degrees of freedom in the doubled Hilbert space \mathcal{H}_2 and $\text{Tr}_{\bar{\Omega}}$ denotes the partial trace over the complementary degrees of freedom. In practice, to compute $S_{\Omega}^{(k)}$ we bipartition the doubled Hilbert space as $\mathcal{H}_2 = \mathcal{H}_{\Omega} \otimes \mathcal{H}_{\bar{\Omega}}$ and perform the Schmidt decomposition of $|k\rangle$,

$$|k\rangle = \sum_{ab} K_{ab}^{(k)} |a\rangle_{\Omega} |b\rangle_{\bar{\Omega}}, \quad (48)$$

where $|a\rangle_{\Omega}$ and $|b\rangle_{\bar{\Omega}}$ are bases of \mathcal{H}_{Ω} and $\mathcal{H}_{\bar{\Omega}}$, respectively. With σ_{ℓ} the singular values of the matrix $K_{ab}^{(k)}$, $\ell = 1, \dots, \min\{\dim(\Omega), \dim(\bar{\Omega})\}$, the EE is given by

$$S_{\Omega}^{(k)} = -\sum_{\ell} \sigma_{\ell}^2 \log \sigma_{\ell}^2. \quad (49)$$

We considered the following two bipartitions of the degrees of freedom, which lead to qualitatively different entanglement patterns:

- The *intersite* partition corresponds to the original bipartition of the $2N$ Majoranas into N L Majoranas and N R Majoranas, $\mathcal{H}_2 = \mathcal{H}^L \otimes \mathcal{H}^R$ (i.e., $\Omega = L$).
- For the *intrasite* partition, we split the L Majoranas into two subsets, $\mathcal{H}^L = \mathcal{H}_A^L \otimes \mathcal{H}_B^L$, where A corresponds to the first $N/2$ Majoranas and B to the last $N/2$ Majoranas, and similarly for \mathcal{H}^R . The Schmidt decomposition is then performed with respect to the bipartition $\mathcal{H}_2 = \mathcal{H}_A \otimes \mathcal{H}_B$ (i.e., $\Omega = A$), where $\mathcal{H}_A = \mathcal{H}_A^L \otimes \mathcal{H}_A^R$ and $\mathcal{H}_B = \mathcal{H}_B^L \otimes \mathcal{H}_B^R$. For a state $|k\rangle$, the decomposition (48) is expressed as

$$|k\rangle = \sum_{i_1 i_2; i_3 i_4} K_{i_1 i_2; i_3 i_4}^{(k)} |i_1 i_3\rangle |i_2 i_4\rangle, \quad (50)$$

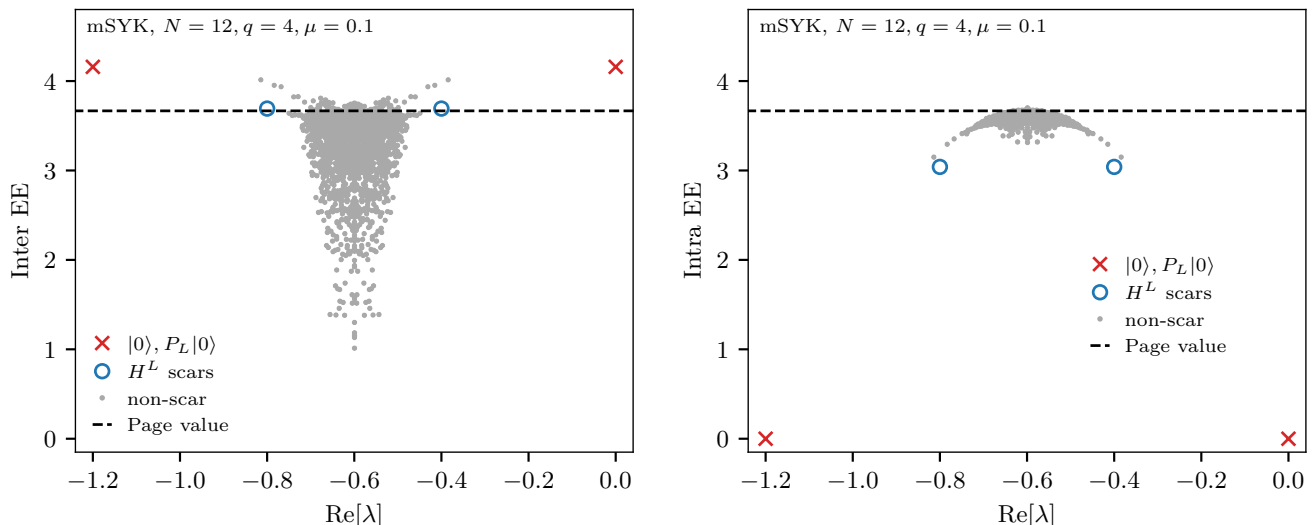


Figure 7. Entanglement entropy Eq. (47) of the eigenstates of one realization of the vectorized Liouvillian of the Majorana SYK model Eq. (4) for $N = 12$, $q = 4$, and $\mu = 0.1$, using two different partitions of the degrees of freedom. Left: Intersite partition corresponding to the original bipartition of $2N$ Majoranas into N L Majoranas and N R Majoranas. Right: Intrasite partition corresponding to a non-contiguous split, see the main text for details. The EE of scars states is sensitive to both the choice of partition and the type of scars. The TFD scar states (red crosses) are clearly differentiated from non-scar states (grey dots) but the H^L scars (blue circles) have an EE that is within the range of the non-scar states.

where $|i_1 i_3\rangle \in \mathcal{H}_A^L \otimes \mathcal{H}_B^L$ and $|i_2 i_4\rangle \in \mathcal{H}_A^R \otimes \mathcal{H}_B^R$ (see Appendix A for more details).

The choice of partition, and hence the calculation of the EE, has implicit a choice of basis (i.e., of representation of the fermion operators and vectorization scheme) which can significantly affect the values of the EE. In particular, the vectorization of Eq. (5) introduces an explicit coupling between the two copies of Hilbert space and therefore, affects the intersite EE. To avoid the extra spurious entanglement, we choose the vectorization of Eq. (13); ultimately, this choice is arbitrary and the most appropriate one must be done on a case-by-case basis.

In Figs. 7 and 8, we show the EE for the dissipative Majorana and complex SYK models, respectively. The EE of many of the non-scar states is close to the Page value (the value for a typical random state),

$$S_{\text{Page}} = \sum_{j=D+1}^{D^2} \frac{1}{j} - \frac{D-1}{2D}, \quad (51)$$

with $D = 2^{N/2}$ the Hilbert space dimension. On the other hand, as expected, the scar states have a different entanglement pattern for the two partitions. This is particularly visible for the complex SYK model because of the higher number of scars induced by the $U(1)$ symmetry. In particular, we see that the scars with high entanglement in one partition have low entanglement in the other. Consider, for example, the states $|0\rangle$ and $P^L|0\rangle$. Since these states correspond to the infinite-temperature TFD and its parity reflection, they

have maximal entanglement between the L and R spaces; correspondingly, the intersite EE reaches the maximum value $\log D = \frac{N}{2} \log 2$. On the other hand, the intrasite EE vanishes for this state (see Appendix A). The other $U(1)$ scars have larger intrasite EE than the TFD or its parity reflection, but it is still noticeably less than that of the bulk of the non-scar states. Since the intrasite EE we consider here coincides with the *operator entanglement entropy* [73–75], this low EE for this partition is an indication of a simple operator complexity. This is no surprise if one looks explicitly into the defining expressions [see Eq. (28)]. By contrast, the definition of the H_L scar does not point to a simple operator complexity. Indeed, its EE is closer to that of non-scar states and in all cases does not vanish.

VI. LINDBLAD SCARS IN SPIN CHAINS

The existence and characterization of Lindblad scars is not exclusive to the dissipative SYK model discussed previously. In this section, we show that similar findings also occur in a dissipative random spin-1/2 XXZ chain whose Hamiltonian is given by

$$\hat{H}_S = -J \sum_{i=1}^N (\hat{X}_i \hat{X}_{i+1} + \hat{Y}_i \hat{Y}_{i+1} + \Delta \hat{Z}_i \hat{Z}_{i+1}) - \sum_{i=1}^N h_i \hat{Z}_i, \quad (52)$$

where \hat{X}_i , \hat{Y}_i , and \hat{Z}_i are the standard Pauli matrices on site i , we have assumed periodic boundary condi-

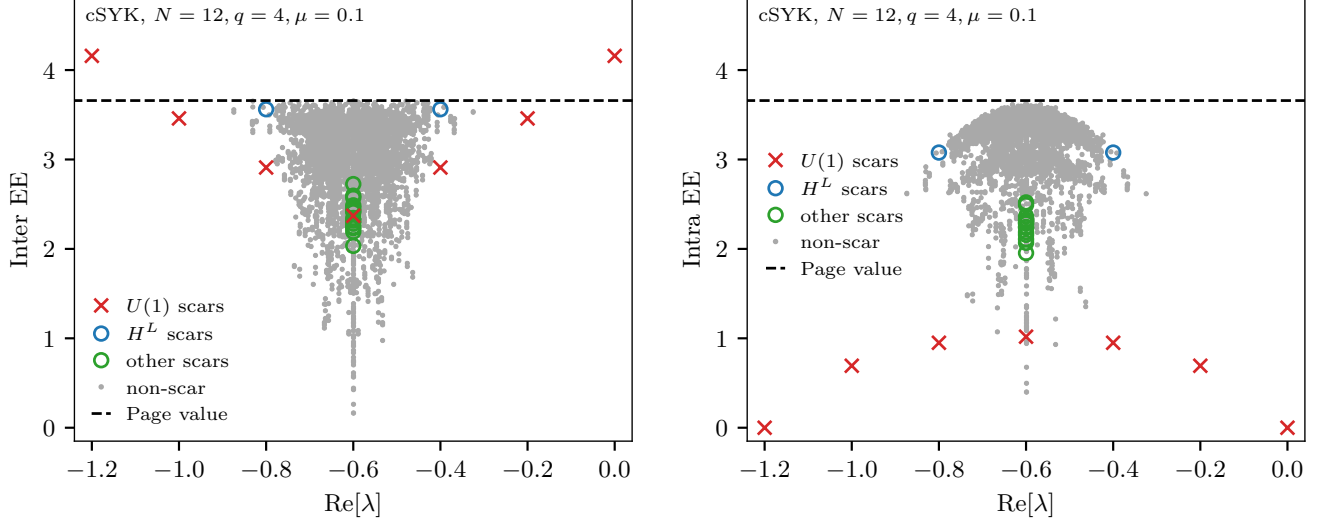


Figure 8. Entanglement entropy Eq. (47) of the eigenstates of one realization of the vectorized Liouvillian of the complex SYK model Eq. (26) for $N = 12$, $q = 4$, and $\mu = 0.1$, using two different partitions of the degrees of freedom. Left: Intersite partition corresponding to the original bipartition of $2N$ Majoranas into N L Majoranas and N R Majoranas. Right: Intrasite partition corresponding to a non-contiguous split, see the main text for details. The EE of scars states (red crosses and green and blue circles) has a broad range of values, from above the Page value typical of a highly entangled random state down to zero entanglement. As in the Majorana case, the EE is sensitive to both the choice of partition and the type of scars. The $U(1)$ scars (red crosses) are only present in the complex SYK model. We also observe that the EE of each of the fifteen degenerate scars that we cannot relate to a symmetry (green circles) is different and does not overlap with the rest of scars, except with one $U(1)$ scar with the same eigenvalue.

tions ($\hat{X}_{N+1} \equiv \hat{X}_1$, etc.), $h_i \in [-h, h]$ are random longitudinal fields and N is the number of sites. When h/J is sufficiently small (large), the model is quantum chaotic (many-body localized) [76]. We set $h/J = 0.5$ and $\Delta = 1.1$ so that the system is in the quantum chaotic phase. The XXZ Hamiltonian also has a $U(1)$ symmetry $[\hat{H}_S, \sum_{i=1}^N \hat{Z}_i] = 0$. We choose the jump operators to be $\hat{L}_i = \hat{X}_i$ so that they break the $U(1)$ symmetry in the Liouvillian. For our calculations we choose $\mu = 0.1$ which corresponds to a much weaker dissipation than in the SYK and complex SYK cases.

The vectorization of the Liouvillian is given by [47, 77, 78]:

$$\mathcal{L} = -i \left(\hat{H}_S \otimes \mathbb{1} - \mathbb{1} \otimes \hat{H}_S^* \right) + \mu \sum_{\alpha} \left[\hat{L}_{\alpha} \otimes \hat{L}_{\alpha}^* - \frac{1}{2} \left(\hat{L}_{\alpha}^{\dagger} \hat{L}_{\alpha} \otimes \mathbb{1} + \mathbb{1} \otimes (\hat{L}_{\alpha}^{\dagger} \hat{L}_{\alpha})^* \right) \right]. \quad (53)$$

Defining

$$X_i^L = \hat{X}_i \otimes \mathbb{1}, \quad X_i^R = \mathbb{1} \otimes \hat{X}_i^*, \quad (54)$$

$$Y_i^L = \hat{Y}_i \otimes \mathbb{1}, \quad Y_i^R = \mathbb{1} \otimes \hat{Y}_i^*, \quad (55)$$

$$Z_i^L = \hat{Z}_i \otimes \mathbb{1}, \quad Z_i^R = \mathbb{1} \otimes \hat{Z}_i^*, \quad (56)$$

we can equivalently write

$$\mathcal{L} = -i \left(H_S^L - H_S^R \right) + H_I, \quad (57)$$

with H_S^L obtained from \hat{H}_S by replacing \hat{X}_i by X_i^L , etc., and

$$H_I = \mu \sum_{i=1}^N X_i^L X_i^R - N\mu. \quad (58)$$

The vectorized Lindbladian has the following discrete symmetries,

$$\left[\prod_k Z_k^L Z_k^R, \mathcal{L} \right] = 0, \quad (59)$$

$$\left[\text{SWAP} \times \prod_k Z_k^L, \mathcal{L} + \mu N \right] = 0, \quad (60)$$

$$\left[\text{SWAP} \times K, \mathcal{L} \right] = 0, \quad (61)$$

where SWAP is the operator that interchanges L and R and K is complex conjugation. Because of Eq. (60), the eigenvalues of $\mathcal{L} + \mu N$ occur in pairs $\{\lambda_k, -\lambda_k\}$, while Eq. (61) implies that they appear as complex conjugate pairs if not real.

Although the operator Eq. (58) resembles H_I of the SYK and complex SYK models, its properties are significantly different. In particular, its ground state is

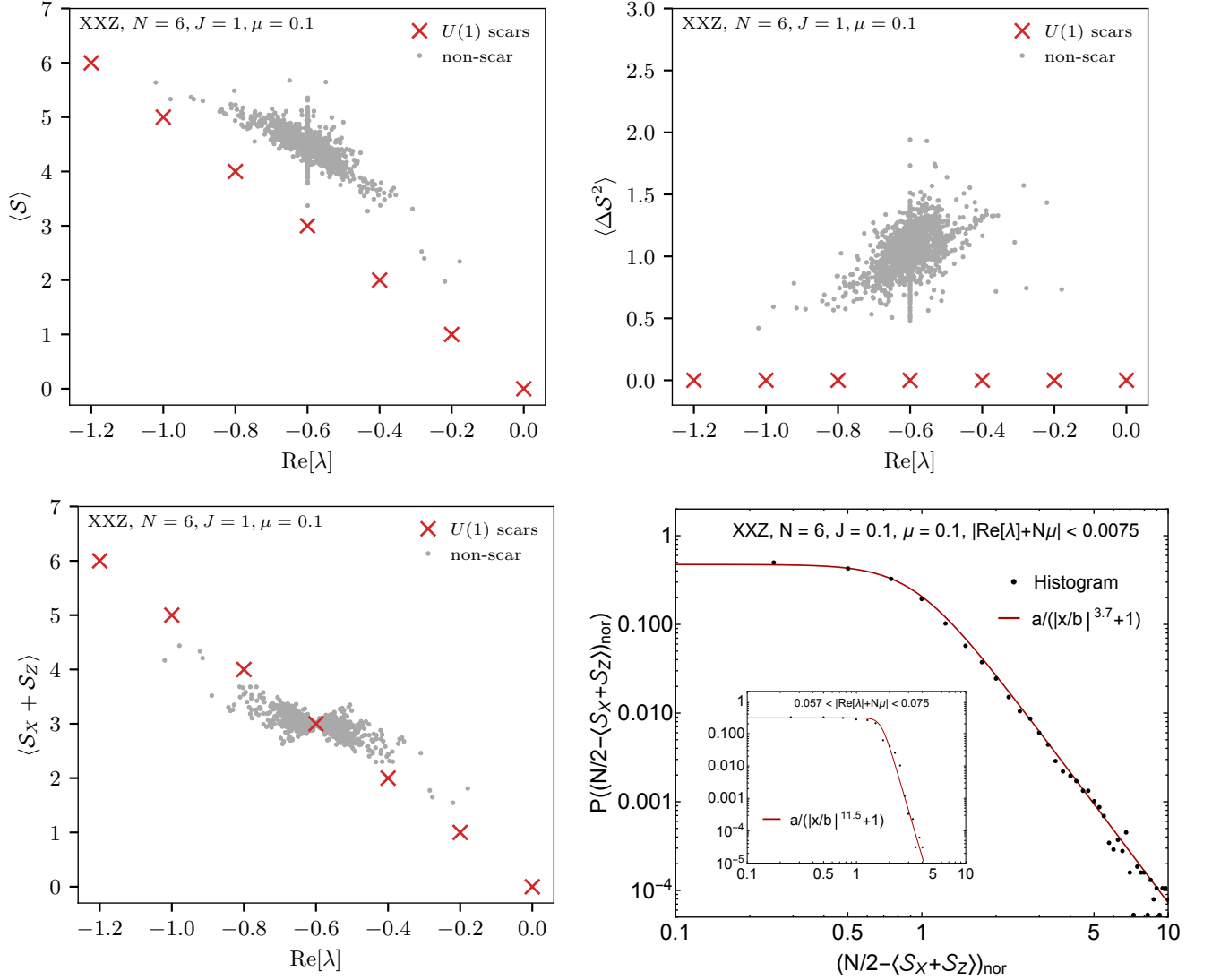


Figure 9. Upper left: Operator size Eq. (66) of scar states (red crosses) and non-scar states (grey dots) for one realization of the $N = 6$ dissipative XXZ model Eq. (52). Upper right: Operator size variance $\Delta S^2 = \langle S^2 \rangle - \langle S \rangle^2$. Lindblad scar states have vanishing size variance since they are shared eigenstates of the Liouvillian and size operator. Lower left: Operator size for Pauli X and Z operators, Eqs. (67) and (69). Scar states have size $-\text{Re}[\lambda]/2\mu$ since they only have components from Z operators so this observable can be used to characterize scar state in this model. Lower right: Log-log plot of histogram of the normalized operator size for Pauli X and Z operators for non-scar states. We observe a similar power-law decay as in the SYK case that suggests deviations from the ETH for dissipative quantum chaotic systems.

2^N fold degenerate, while the ground state of H_I in Eq. (8) is unique. The ground-state degeneracy of H_I is lifted by a nonzero value of J , and the steady state of $-iH_0 + H_I + N\mu$ is only well separated from the rest of the spectrum for sufficiently small values of $\|(H_I + N\mu)\|/\|H_0\|$. This is the case for our choice of $\mu = 0.1$ for which $\|H_I + N\mu\|/\|H_0\| \approx 0.05$ compared to 0.5 for the corresponding ratio for the complex SYK (compare the complex SYK spectrum and the XXZ spectrum in Fig. 1). At this value of μ about 40 percent of the eigenvalues of $\mathcal{L} + N\mu$ are purely imaginary.

Due to the $U(1)$ symmetry that is broken by the jump operators, we expect the presence of $U(1)$ scars. A

straightforward calculation shows that the role of the p -tuple operator $\widehat{\mathcal{N}}_p$ Eq. (28) that generates the scars in the complex SYK model is played by

$$\mathcal{M}_p = \sum_{k_1 \neq k_2 \neq \dots \neq k_p} Z_{k_1} Z_{k_2} \dots Z_{k_p}. \quad (62)$$

Since it verifies the two conditions (i) and (ii'), the scars in the dissipative spin-chain $U(1)$ are $\mathcal{M}_p^L|0\rangle$ with $p = 0, \dots, N/2$, whose eigenvalues are $-2p\mu$:

$$\mathcal{L}\mathcal{M}_p^L|0\rangle = -2p\mu\mathcal{M}_p^L|0\rangle. \quad (63)$$

Unlike in the SYK model, $H^L|0\rangle$ is not a scar because the Hamiltonian has terms with a different number of Pauli matrices: one Pauli matrix in the magnetic field term and two Pauli matrices in the exchange term. This is confirmed by a scatter plot of the eigenvalues, see Fig. 1 (left) where the scar states are shown by the red crosses.

In order to identify and further characterize these scars, we computed the size and the EE. Paralleling the definition introduced in Sec. IV, the size operator of spin systems is given by [79–83]

$$\mathcal{S}(\hat{\mathcal{O}}) = -\frac{1}{4} \sum_{\{\hat{\Sigma}_i\}} \left(\hat{\Sigma}_i \hat{\mathcal{O}} \hat{\Sigma}_i^\dagger - \hat{\mathcal{O}} \right), \quad (64)$$

$$\mathcal{S}_\Sigma(\hat{\mathcal{O}}) = \mathcal{S}(\hat{\mathcal{O}}) + \frac{1}{2} \sum_{i=1}^N (\hat{\Sigma}_i \hat{\mathcal{O}} \hat{\Sigma}_i^\dagger - \hat{\mathcal{O}}) \quad (65)$$

with $\hat{\Sigma}_i \in \{\hat{X}_i, \hat{Y}_i, \hat{Z}_i\}$. \mathcal{S} measures the number of sites in which an operator is one of the Pauli matrices, while \mathcal{S}_Σ measures the number occurrences of a specific Pauli operator Σ only. After vectorization, they can be written as

$$\mathcal{S} = \frac{3N}{4} - \frac{1}{4} \sum_{\Sigma_i} \Sigma_i^L \Sigma_i^R, \quad (66)$$

$$\mathcal{S}_X = \frac{N}{4} - \frac{1}{4} \sum_i^N (-X_i^L X_i^R + Y_i^L Y_i^R + Z_i^L Z_i^R), \quad (67)$$

$$\mathcal{S}_Y = \frac{N}{4} - \frac{1}{4} \sum_i^N (X_i^L X_i^R - Y_i^L Y_i^R + Z_i^L Z_i^R), \quad (68)$$

$$\mathcal{S}_Z = \frac{N}{4} - \frac{1}{4} \sum_i^N (X_i^L X_i^R + Y_i^L Y_i^R - Z_i^L Z_i^R). \quad (69)$$

Unlike in the SYK Lindbladian, the size operator for the spin-chain is not proportional to $H_I = -2\mu(\mathcal{S}_Y + \mathcal{S}_Z)$, so its calculation is of more interest. Indeed, the results depicted in the top panels of Fig. 9 show the existence of the $U(1)$ scars and that their size is markedly different from the non-scar states and also different from those in the SYK model. The variance of the operator size vanishes only for the $U(1)$ scars, so it can be employed to identify scars. As was expected, we do not observe H^L scars. Moreover, we do not observe the degenerate scars reported in the SYK model (green circles).

As in Sec. IV, we define partial size operators similar to the even and odd size operators of the Majorana fermion strings. Since $H_I = -2\mu(\mathcal{S}_Y + \mathcal{S}_Z)$, the expectation value of $\mathcal{S}_Y + \mathcal{S}_Z$ is given by $-\text{Re}[\lambda_k]/2\mu$ with λ_k the eigenvalues of the vectorized Lindblad operator. All combinations of size operators \mathcal{S}_{Σ_i} show a systematic behavior as a function of $\text{Re}[\lambda_k]$ (which is termed secular variation in [69, 70]) as well as a fluctuating contribution. For $\mu = 0.1$ we could not find a linear combination of size operators with a negligible smooth behavior. The combination with the smallest, but still significant, smooth behavior of the

non-scar states is $N/2 - \langle \mathcal{S}_X + \mathcal{S}_Z \rangle = \langle \sum_i Y_i^L Y_i^R \rangle / 2$, see Fig. 9 (lower left). Note that $\langle \mathcal{S}_X + \mathcal{S}_Z \rangle = \langle \mathcal{S}_X - \mathcal{S}_Y \rangle - \langle H_I \rangle / 2\mu$, but $\langle \mathcal{S}_X - \mathcal{S}_Y \rangle$ has a stronger dependence on λ . Because of the symmetry of Eq. (60), $N/2 - \langle \mathcal{S}_X + \mathcal{S}_Z \rangle$ is odd as a function of the real part of the eigenvalues of $\mathcal{L} + N\mu/2$, and thus vanishes when the real part of these eigenvalues is equal to zero, which is the case for about 41 percent of the states. The $U(1)$ scars are a sum of strings of \hat{Z}_i , so naturally, $\langle \mathcal{S}_X \rangle$ and $\langle \mathcal{S}_Y \rangle$ are zero (and their difference is as well) so that $\langle \mathcal{S}_X + \mathcal{S}_Z \rangle = -\text{Re}[\lambda_k]/2\mu$ for these states (red crosses in Fig. 9, bottom left). Therefore, this partial size operator is also suitable to characterize scars.

The bottom right panel of Fig. 9 shows a double-logarithmic plot of the full distribution of the normalized size discussed below in a small window around the center of the spectrum (main) and away from the center (inset). As for the SYK model, see Fig. 6, we find a deviation from the ETH behavior, which predicts a Gaussian distribution. However, according to the ETH, this is the case for an energy window with a negligible smooth behavior [67, 69, 70]. As was already discussed for the complex SYK model, the local dependence of the mean ($M(\lambda)$) and width ($\sigma(\lambda)$) on the eigenvalue λ has to be eliminated if there is a substantial variation over the energy window under consideration. We have studied this dependence on both the real and the imaginary part of λ by partitioning the support of the eigenvalues into 100 bins of equal length, and calculating the mean and width for each bin. We did not find any significant smooth variation on the imaginary part of λ , but there is an order of one smooth dependence on $\text{Re}[\lambda] + \mu N$. In the region $|\text{Re}[\lambda] + \mu N| < 0.2$, where a bin contains at least 1000 eigenvalues (for 1000 realizations), the smooth dependence is obtained by fitting (piecewise) smooth functions, $M(\lambda)$ and $\sigma(\lambda)$, to the values of the mean and width for each bin. For example, for $|\text{Re}[\lambda] + \mu N| < 0.02$, we find $M(\text{Re}[\lambda]) \approx 0.45(\text{Re}[\lambda] - \mu N) + ((\text{Re}[\lambda] - \mu N)/0.092)^3$ and $\sigma(\text{Re}[\lambda]) \approx 0.028 + 5|\text{Re}[\lambda] - \mu N|$. For $|\text{Re}[\lambda] + \mu N| > 0.2$, both the width and the mean show large bin to bin fluctuations and a reliable statistical analysis is not possible. Because the operator $\mathcal{S}_X + \mathcal{S}_Z - N/2$ vanishes at $\text{Re}[\lambda] = -\mu N/2$, to combine the data near this point into one histogram, it is important to normalize the distribution of the sizes to zero mean and unit variance. This can be achieved by considering the normalized expectation value,

$$\langle \mathcal{S}_X + \mathcal{S}_Z \rangle_{\text{nor}} = \frac{\langle \mathcal{S}_X + \mathcal{S}_Z \rangle - M(\text{Re}[\lambda])}{\sigma(\text{Re}[\lambda])}. \quad (70)$$

In Fig. 9 (bottom right), we show the distribution of the normalized sizes for $|\text{Re}[\lambda] + \mu N| < 0.0075$ (main) and $0.057 < |\text{Re}[\lambda] + \mu N| < 0.075$ (inset). Both have power-law tails, with a power that increases significantly away from the center of the spectrum. For the complex SYK model we also found a power law but a much weaker dependence on λ (see Fig. 6). The deviation from Gaussian-

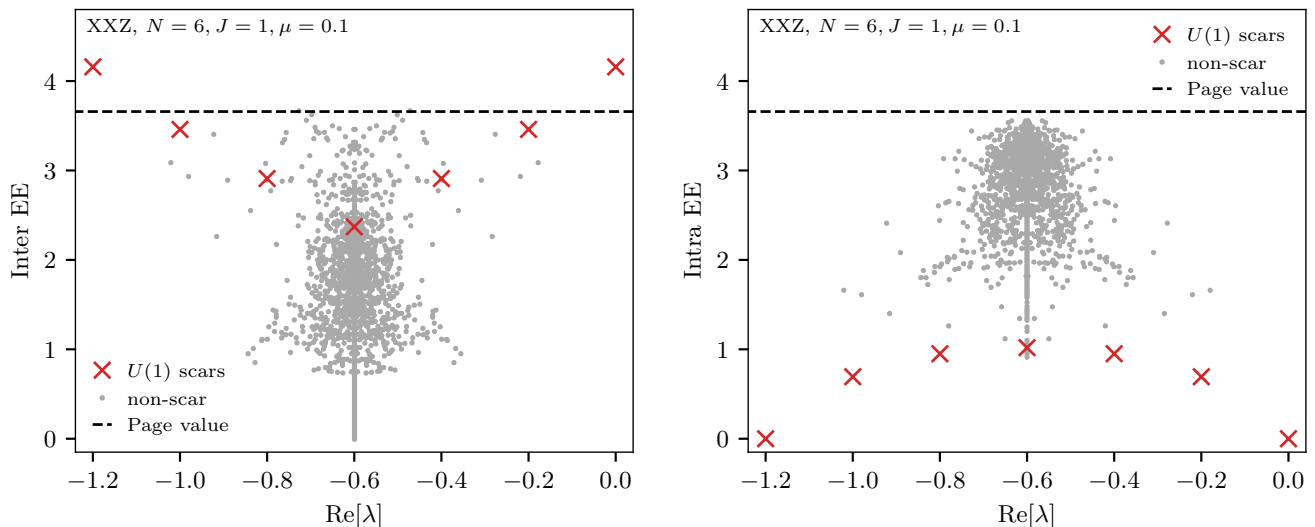


Figure 10. Intersite versus intrasite entanglement entropy Eq. (47) of eigenstates of the Liouvillian for the $N = 6$ XXZ model Eq. (52). Results are qualitatively similar as those for the $U(1)$ scars of the SYK model. In both cases, the scar EE is in general different from the one for non-scar states, covers a relatively large range of values and, is sensitive to the partition.

ity, which persists also after proper rescaling, Eq. (70), suggests that ETH for Lindblad systems, if it applies, is quite different from the Hermitian analogue.

Finally, Fig. 10 shows the EE for the intersite and intrasite partitions. The results agree with the theoretical expectations and are qualitatively similar to those found in the Lindblad SYK model.

VII. CONCLUSION AND OUTLOOK

We have identified conditions for the existence of scarred eigenstates, which we termed Lindblad scars, of the vectorized Liouvillians that describe the dynamics of many-body quantum chaotic systems coupled to a Markovian bath. To illustrate the generality of our results, we have investigated in detail two models: a dissipative SYK model and a dephasing spin chain. In both cases, we constructed the scar states analytically.

An explicit calculation of the operator size has revealed that many-body quantum scars in these two models have an operator size given by the real part of the eigenvalues. Therefore, the size variance vanishes for scars and can be used to identify them. By contrast, non-scarred states show a smooth distribution centered around its average and with a power-like tail, which suggests strong deviations from the ETH in dissipative quantum chaotic systems. We have also observed that the entanglement properties of the many-body scars are to some extent tunable and, for certain partitions, the entanglement entropy of scarred states is close to the Page value, which suggests that these quantum scars are promising candidates to encode and transmit quantum information.

We have found that Lindblad scars can be determined

from the parity or $U(1)$ symmetry of the Hamiltonian and the precise form of the jump operators. Therefore, a similar analysis for supersymmetric SYK models with one or more supercharges, together with a judicious choice of jump operators promises an even richer pattern of Lindblad scars. We have also identified additional scars in the complex SYK model that, to the best of our understanding, are not related to these symmetries.

It would be interesting to explore the precise role of these Lindblad scars in the quantum dynamics. We recall the many-body scars we have identified are not related to revivals because they are purely decaying modes, that is, they have purely real eigenvalues (see Ref. [36] for a recent account of scars with purely imaginary eigenvalues leading to revivals). Another avenue for future research is a more detailed study of the size operator as a probe to characterize the ETH in dissipative many-body chaos for which the assumption of Gaussianity does not seem to apply.

ACKNOWLEDGMENTS

Andrea Pizzi and Frank Schindler are thanked for useful discussions. A. M. G. G. acknowledges support from the National Natural Science Foundation of China (NSFC): Individual Grant No. 12374138, Research Fund for International Senior Scientists No. 12350710180, and National Key R&D Program of China (Project ID: 2019YFA0308603). L. S. was supported by a Research Fellowship from the Royal Commission for the Exhibition of 1851. J. J. M. V. is supported in part by U.S. DOE Grant No. DE-FAG-88FR40388. A. M. G. G., L. S., and J. J. M. V. acknowledge hospitality and sup-

port from the Simons Center for Geometry and Physics and the program “Non-Hermitian topology, geometry and symmetry across physical platforms” where some of the ideas of this paper were developed.

Appendix A: Schmidt decomposition for the intrasite partition

In this appendix we show that also for the intrasite partition the entanglement entropy can be expressed as in Eq. (49), and show that the intrasite EE of the TFD state vanishes..

In this case, a state $|k\rangle$ can be decomposed as (note the ordering of the indices)

$$|k\rangle = \sum_{i_1 i_3; i_2 i_4} K_{i_1 i_2; i_3 i_4} |i_1 i_3\rangle |i_2 i_4\rangle, \quad (\text{A1})$$

where $|i_1 i_3\rangle \in \mathcal{H}_A^L \otimes \mathcal{H}_B^L$ and $|i_2 i_4\rangle \in \mathcal{H}_A^R \otimes \mathcal{H}_B^R$. The singular value decomposition of $K_{i_1 i_3; i_2 i_4}$ is given by

$$K_{i_1 i_2; i_3 i_4} = \sum_{kl} \sigma_{kl} U_{i_1 i_2; kl} V_{kl; i_3 i_4}^\dagger \quad (\text{A2})$$

with σ_{kl} the singular values, and U and V unitary matrices. The matrix elements, $\langle j_1 j_2 | \rho_{\text{red}} | j_1' j_2' \rangle$, of the reduced density matrix $\rho_{\text{red}} = \text{Tr}_B |k\rangle \langle k|$ can be expressed as

$$\begin{aligned} & \sum_{j_3 j_4} \langle j_1 j_3; j_2 j_4 | k \rangle \langle k | j_1' j_3'; j_2' j_4' \rangle \\ &= \sum_{kl; k' l'} \sum_{j_3 j_4} \sigma_{kl} U_{j_1 j_2; kl} V_{kl; j_3 j_4}^\dagger \sigma_{k' l'} U_{j_1' j_2'; k' l'}^* V_{k' l'; j_3 j_4}^T \\ &= \sum_{kl} \sigma_{kl}^2 U_{j_1 j_3; kl} U_{j_1' j_3'; kl}^* \end{aligned} \quad (\text{A3})$$

where in the last equality we used the unitarity of V . The reduced density matrix is then given by

$$\begin{aligned} \rho_{\text{red}} &= \sum_{kl} \sum_{j_1 j_2; j_1' j_2'} \sigma_{kl}^2 U_{j_1 j_2; kl} U_{j_1' j_2'; kl}^* |j_1 j_2\rangle \langle j_1' j_2'| \\ &= \sum_{kl} \sigma_{kl}^2 |kl\rangle \langle kl| \end{aligned} \quad (\text{A4})$$

with

$$|kl\rangle = \sum_{j_1 j_2} U_{kl; j_1 j_2}^T |j_1 j_2\rangle. \quad (\text{A5})$$

This shows that also for the intrasite partition the reduced density matrix is given by Eq. (49).

Finally, let us use this to calculate the EE of the state $|0\rangle$. Since this state correspond to the infinite temperature TFD, it has maximal entanglement between the L and R spaces; correspondingly, the intersite EE reaches the maximum value $\log D = \frac{N}{2} \log 2$. If the TFD state,

$$|0\rangle = \sum_{i_1 i_2; i_1 i_2} |i_1 i_2\rangle |i_1 i_2\rangle / \sqrt{D} \in \mathcal{H}^L \otimes \mathcal{H}^R, \quad (\text{A6})$$

is expanded according to the intrasite partition (50),

$$|0\rangle = \sum_{i_1 i_2; i_3 i_4} K_{i_1 i_2; i_3 i_4}^{\text{intra}} |i_1 i_3\rangle |i_2 i_4\rangle, \quad (\text{A7})$$

only the matrix elements $K_{i_1 i_2; i_3 i_4}^{\text{intra}} = 1/\sqrt{D}$ are nonzero. This is a projection matrix with only one nonzero singular value resulting in a vanishing intrasite EE as found numerically in Fig. 10. Note that the argument has to be modified for parity reflected TFD state, $P^L|0\rangle$, which has to be perpendicular to the TFD state.

-
- [1] E. J. Heller, Bound-State Eigenfunctions of Classically Chaotic Hamiltonian Systems: Scars of Periodic Orbits, *Phys. Rev. Lett.* **53**, 1515 (1984).
- [2] Z. Ge, A. M. Graf, J. Keski-Rahkonen, S. Slizovskiy, P. Polizogopoulos, T. Taniguchi, K. Watanabe, R. Van Haren, D. Lederman, V. I. Fal’ko, E. J. Heller, and J. Velasco Jr, Direct visualization of relativistic quantum scars in graphene quantum dots, *Nature* **635**, 841 (2024).
- [3] B. Evrard, A. Pizzi, S. I. Mistakidis, and C. B. Dag, Quantum Scars and Regular Eigenstates in a Chaotic Spinor Condensate, *Phys. Rev. Lett.* **132**, 020401 (2024).
- [4] B. Evrard, A. Pizzi, S. I. Mistakidis, and C. B. Dag, Quantum many-body scars from unstable periodic orbits, *Phys. Rev. B* **110**, 144302 (2024).
- [5] A. Pizzi, B. Evrard, C. B. Dag, and J. Knolle, Quantum scars in many-body systems, [arXiv:2408.10301](https://arxiv.org/abs/2408.10301) (2024).
- [6] A. M. Graf, J. Keski-Rahkonen, M. Xiao, S. Atwood, Z. Lu, S. Chen, and E. J. Heller, Birthmarks: Ergodicity Breaking Beyond Quantum Scars, [arXiv:2412.02982](https://arxiv.org/abs/2412.02982) (2024).
- [7] A. Pizzi, Quantum trails and memory effects in the phase space of chaotic quantum systems, [arXiv:2412.04310](https://arxiv.org/abs/2412.04310) (2024).
- [8] Z. Lu, A. M. Graf, E. J. Heller, J. Keski-Rahkonen, and C. B. Dag, Anti-scarring from eigenstate stacking in a chaotic spinor condensate, [arXiv preprint arXiv:2501.17856](https://arxiv.org/abs/2501.17856) (2025).
- [9] Q. Hummel, K. Richter, and P. Schlagheck, Genuine many-body quantum scars along unstable modes in bose-hubbard systems, *Phys. Rev. Lett.* **130**, 250402 (2023).
- [10] M. Serbyn, D. A. Abanin, and Z. Papić, Quantum many-body scars and weak breaking of ergodicity, *Nat. Phys.* **17**, 675–685 (2021).
- [11] H. Bernien, S. Schwartz, A. Keesling, H. Levine, A. Omran, H. Pichler, S. Choi, A. S. Zibrov, M. Endres, M. Greiner, V. Vuletić, and M. D. Lukin, Probing many-body dynamics on a 51-atom quantum simulator, *Nature* **551**, 579–584 (2017).
- [12] D. Bluvstein, A. Omran, H. Levine, A. Keesling, G. Semeghini, S. Ebadi, T. T. Wang, A. A. Michailidis, N. Maskara, W. W. Ho, S. Choi, M. Serbyn, M. Greiner,

- V. Vuletić, and M. D. Lukin, Controlling quantum many-body dynamics in driven rydberg atom arrays, *Science* **371**, 1355–1359 (2021).
- [13] C. J. Turner, A. A. Michailidis, D. A. Abanin, M. Serbyn, and Z. Papić, Weak ergodicity breaking from quantum many-body scars, *Nat. Phys.* **14**, 745–749 (2018).
- [14] K. Pakrouski, P. N. Pallegar, F. K. Popov, and I. R. Klebanov, Many-Body Scars as a Group Invariant Sector of Hilbert Space, *Phys. Rev. Lett.* **125**, 230602 (2020).
- [15] M. Sporre, J. J. M. Verbaarschot, and I. Zahed, Solution of the three anyon problem, *Phys. Rev. Lett.* **67**, 1813 (1991).
- [16] M. Sporre, J. J. M. Verbaarschot, and I. Zahed, Four anyons in a harmonic well, *Phys. Rev. B* **46**, 5738 (1992).
- [17] M. Sporre, J. J. M. Verbaarschot, and I. Zahed, Anyon spectra and the third virial coefficient, *Nucl. Phys. B* **389**, 645 (1993).
- [18] Y.-S. Wu, Multiparticle Quantum Mechanics Obeying Fractional Statistics, *Phys. Rev. Lett.* **53**, 111 (1984).
- [19] M. A. Shifman and A. V. Turbiner, Quantal Problems With Partial Algebraization of the Spectrum, *Commun. Math. Phys.* **126**, 347 (1989).
- [20] M. A. Shifman, Quasiexactly solvable spectral problems, in *XXVIII Cracow School of Theoretical Physics* (1998).
- [21] N. Shiraishi and T. Mori, Systematic Construction of Counterexamples to the Eigenstate Thermalization Hypothesis, *Phys. Rev. Lett.* **119**, 030601 (2017).
- [22] S. Moudgalya, S. Rachel, B. A. Bernevig, and N. Regnault, Exact excited states of nonintegrable models, *Phys. Rev. B* **98**, 235155 (2018).
- [23] I.-C. Chen, B. Burdick, Y. Yao, P. P. Orth, and T. Iadecola, Error-mitigated simulation of quantum many-body scars on quantum computers with pulse-level control, *Physical Review Research* **4**, 043027 (2022).
- [24] H. Cao, D. G. Angelakis, and D. Leykam, Unsupervised learning of quantum many-body scars using intrinsic dimension, *Mach. Learn.: Sci. Technol.* **5**, 025049 (2024).
- [25] G. Ramírez, J. Rodríguez-Laguna, and G. Sierra, Entanglement over the rainbow, *J. Stat. Mech.: Theor. Exper.* **2015**, P06002 (2015).
- [26] C. M. Langlett, Z.-C. Yang, J. Wildeboer, A. V. Gorshkov, T. Iadecola, and S. Xu, Rainbow scars: From area to volume law, *Phys. Rev. B* **105**, L060301 (2022).
- [27] H. Dong, J.-Y. Desaulles, Y. Gao, N. Wang, Z. Guo, J. Chen, Y. Zou, F. Jin, X. Zhu, P. Zhang, H. Li, Z. Wang, Q. Guo, J. Zhang, L. Ying, and Z. Papić, Disorder-tunable entanglement at infinite temperature, *Sci. Adv.* **9**, eadj3822 (2023).
- [28] S. Moudgalya, B. A. Bernevig, and N. Regnault, Quantum many-body scars and Hilbert space fragmentation: a review of exact results, *Rep. Prog. Phys.* **85**, 086501 (2022).
- [29] H.-P. Breuer and F. Petruccione, *The Theory of Open Quantum Systems* (Oxford University Press, Oxford, 2002).
- [30] Q. Chen, S. A. Chen, and Z. Zhu, Weak ergodicity breaking in non-Hermitian many-body systems, *SciPost Phys.* **15**, 052 (2023).
- [31] R. Shen, F. Qin, J.-Y. Desaulles, Z. Papić, and C. H. Lee, Enhanced Many-Body Quantum Scars from the Non-Hermitian Fock Skin Effect, *Phys. Rev. Lett.* **133**, 216601 (2024).
- [32] M. de Leeuw, C. Paletta, B. Pozsgay, and E. Vernier, Hidden quasilocal charges and Gibbs ensemble in a Lindblad system, *Phys. Rev. B* **109**, 054311 (2024).
- [33] S. Maity and R. Hamazaki, Kinetically constrained models constructed from dissipative quantum dynamics, *Phys. Rev. B* **110**, 014301 (2024).
- [34] A. Teretenkov and O. Lyckkovskiy, Duality between open systems and closed bilayer systems: Thermofield double states as quantum many-body scars, *Phys. Rev. B* **110**, L241105 (2024).
- [35] H.-R. Wang, D. Yuan, S.-Y. Zhang, Z. Wang, D.-L. Deng, and L.-M. Duan, Embedding Quantum Many-Body Scars into Decoherence-Free Subspaces, *Phys. Rev. Lett.* **132**, 150401 (2024).
- [36] X.-P. Jiang, M. Xu, X. Yang, Y. Wang, and L. Pan, Robustness of quantum many-body scars in the presence of Markovian bath, [arXiv:2501.00886](https://arxiv.org/abs/2501.00886) (2025).
- [37] A. M. García-García, L. Sá, and J. J. M. Verbaarschot, Universality and its limits in non-Hermitian many-body quantum chaos using the Sachdev-Ye-Kitaev model, *Phys. Rev. D* **107**, 066007 (2023).
- [38] G. Cipolloni and J. Kudler-Flam, Non-Hermitian Hamiltonians violate the eigenstate thermalization hypothesis, *Phys. Rev. B* **109**, L020201 (2024).
- [39] Y. Mao, P. Zhong, H. Lin, X. Wang, and S. Hu, Diagnosing Thermalization Dynamics of Non-Hermitian Quantum Systems via GKSL Master Equations, *Chin. Phys. Lett.* **41**, 070301 (2024).
- [40] S. S. Roy, S. Bandyopadhyay, R. C. de Almeida, and P. Hauke, Unveiling Eigenstate Thermalization for Non-Hermitian systems, [arXiv:2309.00049](https://arxiv.org/abs/2309.00049) (2023).
- [41] R. Hamazaki, M. Nakagawa, T. Haga, and M. Ueda, Lindbladian Many-Body Localization, [arXiv:2206.02984](https://arxiv.org/abs/2206.02984) (2022).
- [42] G. Almeida, P. Ribeiro, H. M., and L. Sá, Universality, Robustness, and Limits of the Eigenstate Thermalization Hypothesis in Open Quantum Systems, In preparation (2025).
- [43] L. Sá, P. Ribeiro, and T. Prosen, Lindbladian dissipation of strongly-correlated quantum matter, *Phys. Rev. Res.* **4**, L022068 (2022).
- [44] A. Kulkarni, T. Numasawa, and S. Ryu, Lindbladian dynamics of the Sachdev-Ye-Kitaev model, *Phys. Rev. B* **106**, 075138 (2022).
- [45] A. M. García-García, L. Sá, J. J. M. Verbaarschot, and J. P. Zheng, Keldysh wormholes and anomalous relaxation in the dissipative Sachdev-Ye-Kitaev model, *Phys. Rev. D* **107**, 106006 (2023).
- [46] K. Kawabata, A. Kulkarni, J. Li, T. Numasawa, and S. Ryu, Dynamical quantum phase transitions in Sachdev-Ye-Kitaev Lindbladians, *Phys. Rev. B* **108**, 075110 (2023).
- [47] K. Kawabata, A. Kulkarni, J. Li, T. Numasawa, and S. Ryu, Symmetry of Open Quantum Systems: Classification of Dissipative Quantum Chaos, *PRX Quantum* **4**, 030328 (2023).
- [48] A. M. García-García, L. Sá, J. J. M. Verbaarschot, and C. Yin, Toward a classification of PT-symmetric quantum systems: From dissipative dynamics to topology and wormholes, *Phys. Rev. D* **109**, 105017 (2024).
- [49] O. Bohigas and J. Flores, Two-body random Hamiltonian and level density, *Phys. Lett. B* **34**, 261 (1971).
- [50] J. French and S. Wong, Validity of random matrix theories for many-particle systems, *Phys. Lett. B* **33**, 449 (1970).
- [51] J. B. French and S. S. M. Wong, Some random-matrix

- level and spacing distributions for fixed-particle-rank interactions, *Phys. Lett. B* **35**, 5 (1971).
- [52] A. Gervois, Level densities for random one- or two-body potentials, *Nucl. Phys. A* **184**, 507 (1972).
- [53] S. Sachdev and J. Ye, Gapless spin-fluid ground state in a random quantum Heisenberg magnet, *Phys. Rev. Lett.* **70**, 3339 (1993).
- [54] L. Benet and H. A. Weidenmüller, Review of the k -body embedded ensembles of Gaussian random matrices, *J. Phys. A* **36**, 3569 (2003).
- [55] A. Kitaev, [A simple model of quantum holography](#) (2015), string seminar at KITP and Entanglement 2015 program, 12 February, 7 April and 27 May 2015, <http://online.kitp.ucsb.edu/online/entangled15/>.
- [56] J. Maldacena and D. Stanford, Remarks on the Sachdev-Ye-Kitaev model, *Phys. Rev. D* **94**, 106002 (2016).
- [57] J. Maldacena, S. H. Shenker, and D. Stanford, A bound on chaos, *J. High Energy Phys.* **2016**, 106 (2016).
- [58] A. M. García-García and J. J. M. Verbaarschot, Spectral and thermodynamic properties of the Sachdev-Ye-Kitaev model, *Phys. Rev. D* **94**, 126010 (2016).
- [59] G. Lindblad, On the generators of quantum dynamical semigroups, *Commun. Math. Phys.* **48**, 119 (1976).
- [60] V. Gorini, A. Kossakowski, and E. C. G. Sudarshan, Completely positive dynamical semigroups of N -level systems, *J. Math. Phys.* **17**, 821 (1976).
- [61] L. M. Sieberer, M. Buchhold, and S. Diehl, Keldysh field theory for driven open quantum systems, *Rep. Prog. Phys.* **79**, 096001 (2016).
- [62] J. Maldacena, G. J. Turiaci, and Z. Yang, Two dimensional nearly de Sitter gravity, *J. High Energy Phys.* **2021**, 139 (2021).
- [63] A. M. García-García, Y. Jia, D. Rosa, and J. J. M. Verbaarschot, Sparse Sachdev-Ye-Kitaev model, quantum chaos, and gravity duals, *Phys. Rev. D* **103**, 106002 (2021).
- [64] J. Maldacena, Eternal black holes in anti-de Sitter, *J. High Energy Phys.* **4**, 021 (2003).
- [65] Y. Gu, A. Kitaev, S. Sachdev, and G. Tarnopolsky, Notes on the complex Sachdev-Ye-Kitaev model, *J. High Energy Phys.* **2020**, 157 (2020).
- [66] B. Buča and T. Prosen, A note on symmetry reductions of the Lindblad equation: transport in constrained open spin chains, *New J. Phys.* **14**, 073007 (2012).
- [67] M. Srednicki, Chaos and quantum thermalization, *Phys. Rev. E* **50**, 888 (1994).
- [68] J. M. Deutsch, Quantum statistical mechanics in a closed system, *Phys. Rev. A* **43**, 2046 (1991).
- [69] J. P. Draayer, J. B. French, and S. S. M. Wong, Strength distributions and statistical spectroscopy. I. General theory, *Ann. Phys.* **106**, 472 (1977).
- [70] J. P. Draayer, J. B. French, and S. S. M. Wong, Strength distributions and statistical spectroscopy ii. shell-model comparisons, *Ann. Phys.* **106**, 503 (1977).
- [71] J. J. M. Verbaarschot and P. J. Brussaard, Fixed-JT averages of electromagnetic operators, *Nucl. Phys. A* **423**, 77 (1984).
- [72] J. J. M. Verbaarschot and P. J. Brussaard, Distribution of electromagnetic transition amplitudes, *Z. Phys. A* **321**, 125 (1985).
- [73] T. Prosen and I. Pižorn, Operator space entanglement entropy in a transverse Ising chain, *Phys. Rev. A* **76**, 032316 (2007).
- [74] T. Zhou and D. J. Luitz, Operator entanglement entropy of the time evolution operator in chaotic systems, *Phys. Rev. B* **95**, 094206 (2017).
- [75] D. Wellnitz, G. Preisser, V. Alba, J. Dubail, and J. Schachenmayer, Rise and Fall, and Slow Rise Again, of Operator Entanglement under Dephasing, *Phys. Rev. Lett.* **129**, 170401 (2022).
- [76] D. J. Luitz, N. Laflorencie, and F. Alet, Many-body localization edge in the random-field Heisenberg chain, *Phys. Rev. B* **91**, 081103 (2015).
- [77] L. Sá, P. Ribeiro, and T. Prosen, Complex Spacing Ratios: A Signature of Dissipative Quantum Chaos, *Phys. Rev. X* **10**, 021019 (2020).
- [78] L. Sá, P. Ribeiro, and T. Prosen, Symmetry Classification of Many-Body Lindbladians: Tenfold Way and Beyond, *Phys. Rev. X* **13**, 031019 (2023).
- [79] D. A. Roberts, D. Stanford, and A. Streicher, Operator growth in the SYK model, *J. High Energy Phys.* **2018**, 6 (2018).
- [80] X.-L. Qi, E. J. Davis, A. Periwai, and M. Schleier-Smith, Measuring operator size growth in quantum quench experiments, [arXiv:1906.00524](#) (2019).
- [81] X.-L. Qi and A. Streicher, Quantum epidemiology: operator growth, thermal effects, and SYK, *J. High Energy Phys.* **2019**, 12 (2019).
- [82] T. Schuster, B. Kobrin, P. Gao, I. Cong, E. T. Khabiboulline, N. M. Linke, M. D. Lukin, C. Monroe, B. Yoshida, and N. Y. Yao, Many-Body Quantum Teleportation via Operator Spreading in the Traversable Wormhole Protocol, *Phys. Rev. X* **12**, 031013 (2022).
- [83] T. Schuster and N. Y. Yao, Operator Growth in Open Quantum Systems, *Phys. Rev. Lett.* **131**, 160402 (2023).